Report No. CG-D-09-98

Investigation of a Multi-Sensor Method to Map Oil Spill Thickness

G. L. Hover

U.S. Coast Guard
Research and Development Center
1082 Shennecossett Road
Groton, CT 06340-6096

Robert Shemo
J. Thomas Parr

TASC, Inc.
55 Walkers Brook Drive
Reading, MA 01867

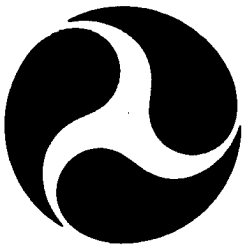

Final Report
December 1997

Prepared for:

U.S. Department of Transportation
United States Coast Guard
Marine Safety and Environmental Protection, (G-M)
Washington, DC 20593-0001

NOTICE

This document is disseminated under the sponsorship of the Department of Transportation in the interest of information exchange. The United States Government assumes no liability for its contents or use thereof.

The United States Government does not endorse products or manufacturers. Trade or manufacturers' names appear herein solely because they are considered essential to the object of this report.

The contents of this report reflect the views of the Coast Guard Research & Development Center. This report does not constitute a standard, specification, or regulation.

Marc B. Mandler
Technical Director
United States Coast Guard
Research & Development Center
1082 Shennecossett Road
Groton, CT 06340-6096

ACKNOWLEDGEMENTS

This work was performed under the supervision of the U.S. Coast Guard Research and Development Center, Groton, CT, as part of its Comprehensive Marine Environmental Response project. The project officer for this task was Mr. Gary Hover of the Maritime Operations Technology Division. The Remote Sensing/Geographic Information Center (RSGISC) of the U.S. Army Corps of Engineers has supported this research with partial funding under its Oil Spill Research Program. The Oil Spill Research Program was directed by Dr. Ike McKim, managed by Major Bruce Gwilliam, and evaluated by Dr. Robert Bolus, all of the RSGISC at CRREL in Hanover, New Hampshire, using OPA 90 funds. Mr. John Putukian of the U.S. Department of Transportation's Volpe National Transportation Systems Center served as the Technical Task Initiator for the contract with TASC.

The Frequency-Scanning Radiometer (FSR) oil thickness sensor was developed by MIT Lincoln Laboratory under joint sponsorship from the U.S. Coast Guard Research and Development Center and the U.S. Minerals Management Service (MMS). The principal Lincoln Laboratory investigators were Mr. Thomas Murphy, Mr. Oliver McMahon, and Dr. Elliot Brown. The MMS contract manager was Mr. James Lane.

[BLANK]

TABLE OF CONTENTS

TABLE OF CONTENTS (Continued)

LIST OF FIGURES

Figure **Page**

LIST OF TABLES

Table **Page**

EXECUTIVE SUMMARY

Presently, maritime oil spill response and pollution deterrence forces have no reliable means of mapping oil slick thickness volume from the air. This report describes a technology demonstration and preliminary evaluation of a multi-sensor method that might provide such a capability.

During September 1996, the U.S. Coast Guard Research and Development Center and its contractor, TASC, worked with the M.I.T. Lincoln Laboratory and the U.S. Minerals Management Service to test a new multi-sensor concept for monitoring oil spills. The test was conducted at the OHMSETT National Oil Spill Response Test Facility in Leonardo, New Jersey. Data were collected with a prototype frequency scanning microwave radiometer (FSR) and a commercial thermal infrared (IR) imaging radiometer. The multi-sensor method used FSR-derived oil thickness estimates to calibrate the gray scale of infrared images, thereby providing a means of producing oil thickness maps and volume estimates over relatively large areas. The target set consisted of containment rings filled with various known thicknesses of several oils, including both crude and diesel.

Given a particular set of environmental conditions, the temperatures observed by an infrared imager are a function of oil thickness and type, but absolute thickness cannot be determined from the IR data alone; only a relative thickness estimate is possible. The OHMSETT experiment was designed to test whether the FSR data could be used to provide a calibration for the IR imagery, allowing the derivation of thickness maps and volume estimates for an entire oil spill.

Analysis of data from this test demonstrated that if measurements from both sensors are obtained closely in time in relatively low sea states, the proposed method may be capable of providing a reliable oil thickness mapping capability. Tests conducted under simulated wind, wave, and chop conditions generally produced weaker correlations, as did tests where calibration of the IR imagery with FSR data occurred over many minutes.

While environmental factors may impose some operational constraints, it appears that the FSR/IR oil spill-monitoring concept tested at OHMSETT merits future consideration by the Coast Guard, particularly for low sea-state applications. Further FSR/IR system development and testing at OHMSETT would be required prior to any airborne demonstrations. The objectives of these new tests would be to develop an understanding of how environmental factors impact the surface temperature of the oil, to determine improved methods for instrument calibration, and to produce a more closely integrated FSR/IR system consistent with efficient, safe, and reliable operation on board a helicopter.

To aid in eventual development of an airborne sensor, a number of mechanical, electrical, and system/operational issues are discussed. These issues should be considered in the design of a well-integrated and truly effective oil spill monitoring system.

1. INTRODUCTION

Determining the extent and volume of an oil spill is important information to aid in selecting the best cleanup response for an accident. Under U.S. Coast Guard and U.S. Minerals Management Service sponsorship, MIT's Lincoln Laboratory (MIT/LL) has constructed a Frequency Scanning Radiometer (FSR) which can estimate the thickness of an oil film on water (Refs.1 through 3). Infrared (IR) imagery can be used to determine the relative thickness of oil on water. The US Coast Guard is interested in the feasibility of combining these technologies to produce maps of oil spill thickness and volume to aid in cleanup operations.

1.1 BACKGROUND

Several studies have been performed using thermal infrared sensing to detect and estimate the relative thickness of oil spills (Refs. 4 through 6). These studies indicate that IR has been reasonably successful in the detection of oil slicks due to the differences in the emissivity and specific heat of the oil and water. Under isothermal conditions the temperature of the oil usually appears to be lower than the temperature of the water. Under conditions where solar insolation is occurring and the oil is sufficiently thick (greater than 0.5 mm), the oil heats up faster than the water and appears warmer (Ref. 7).

As oil thickness, condition and local environmental conditions vary, the oil slick's thermal signature appears different. Both thick oil and emulsions can appear warmer than the surrounding water. Oil sheens may appear cooler than the surrounding water. Fresh oil spills where the volatiles are evaporating rapidly can also appear cooler than the surrounding water (Ref. 8). In addition, these temperature differences all vary due to the effects of the local environment. These effects on the thermal signature of the oil spill will be discussed in detail later in this report.

Using IR to detect oil spills has several advantages over other methods such as active radar, visible and ultraviolet systems (Refs. 7 and 8):

- Instantaneous areal coverage is provided by IR imaging devices
- Interpretation of the imagery is straightforward
- IR systems are able to detect relative thickness of the oil
- IR systems are easily mounted in an aircraft and consume minimal power
- Operation is possible during day or night
- IR systems are reasonably priced.

There are also several disadvantages to using IR technology for oil spill detection:

- Measurement of absolute oil thickness is not possible
- Operation is not possible above cloud cover
- When used in conjunction with cleanup methods using dispersants, the image becomes difficult to interpret because of the changes to the oil's properties caused by the dispersants
- IR systems must be mounted so that a window does not obstruct the view.

An integrated FSR and thermal IR system has the potential to overcome the limitations of each of these detector systems operating alone. In contrast to the thermal IR imaging radiometer, the MIT/LL FSR measures the microwave brightness temperature of oil-covered water over a range of frequencies. The measurements are processed to estimate the thickness of the oil, but provide only a point value associated with the relatively narrow field-of-view for the FSR antenna (Ref. 1). The FSR measurement process is relatively time consuming, and due to the dynamic nature of an oil slick and the environmental factors affecting it, it would not be feasible to use the FSR alone to provide broad area monitoring of oil slick thicknesses. However, it may be feasible to use the absolute measurement capability of the FSR to calibrate the thermal IR imagery, allowing areal thickness estimates to be determined from the observed oil slick surface temperatures.

1.2 OBJECTIVE

The objective of this study is to determine the feasibility of using an FSR to calibrate the relative thickness gradients detected in a thermal infrared image of an oil spill. Using this

calibration, thickness maps of selected oil targets are produced using the determined relationship between FSR defined thickness and the thermal signature of the oil. In principle, these thickness maps can then be integrated over the area surveyed to produce an estimate of the total volume of oil on the water surface. The feasibility of an operational airborne FSR/IR system is considered and recommendations for future experiments and implementation of this system are made.

1.3 DOCUMENT OVERVIEW

This Final Report presents results obtained from the FSR/IR data collected in September 1996 at the OHMSETT Test Facility. The technical approach, including details of the infrared instrumentation and data collection and analysis procedures, is discussed in Section 2. Test results are presented in Section 3 and recommendations for future testing and implementation of an operational FSR/IR instrument are discussed in Section 4. Our conclusions, based upon the OHMSETT experiment, are found in Section 5. The Appendices contain complete graphical data for each of the test series.

[BLANK]

2. TECHNICAL APPROACH

This study consisted of two distinct phases. During the data collection phase, the infrared imager was obtained, data collection procedures were coordinated with Lincoln Laboratory and TASC determined a means of boresighting the FSR and IR imager using a CO_2 laser. Data collection was then performed at the OHMSETT test tank. The second phase consisted of data reduction and analysis. FSR and environmental data were obtained from Lincoln Laboratory and OHMSETT, and correlated with the IR imagery.

2.1 EQUIPMENT

The data collection required the use of a prototype FSR developed by MIT Lincoln Laboratory, which is described in Reference 1, and an infrared imager. The FSR is a multi-frequency passive microwave radiometer capable of estimating the thickness of oil films on water under most weather conditions. This measurement is accomplished by sampling the brightness temperatures across selected microwave frequencies and comparing the resulting brightness temperature versus frequency curves with theoretical curves which correspond to specific oil thicknesses (Ref. 1). An infrared imaging radiometer was used by TASC to collect thermal images of the oil targets that were measured by the FSR. TASC rented an Inframetrics 760 infrared imaging radiometer, shown in Figure 1 (Ref. 5), to perform the thermal data collection.

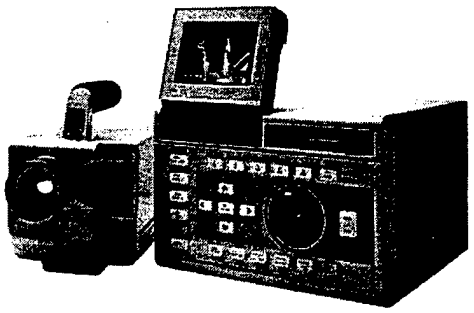

Figure 1. Inframetrics 760 Infrared Imaging Radiometer

The Inframetrics 760 is sensitive in the 8-12 μm range. This instrument provides 256 levels in temperature ranges from 2°K to 1000°K and has ±2% or ±2°K accuracy with a

repeatability of ±0.5% or ±0.5°K. The field-of-view of this instrument is 20 degrees in the horizontal and 15 degrees in the vertical. The output from this instrument is a TIFF image that is captured on an IBM formatted floppy diskette. One diskette can hold 25 images and the image directory (Ref. 9).

2.2 TEST FACILITY AND SETUP

The collection of FSR/IR data occurred at the Minerals Management Service's OHMSETT National Oil Spill Response Test Facility in Leonardo, NJ, during September 10-19, 1996. Several test conditions and oils were desired to determine the applicability and robustness of the instrumentation for different environments and oils. Both day and night testing of diesel and crude oils were performed. Fans mounted alongside the containment rings were available to produce a thickness gradient across the pools. The wave generator was used to determine the effect of waves on the instrumentation. The test tank at OHMSETT was outfitted with five-meter diameter containment rings as shown in Figure 2. For each test a calculated volume of oil was poured into each containment ring to produce the desired *average* thickness. It is important to note that, except in very calm conditions, the actual thickness of the oil varied considerably within each ring. The thickness in each ring for the five test periods is shown Table 1.

Over the test tank there is a moveable bridge that is able to travel over the containment rings. The FSR and IR detectors were set up on this bridge as shown in Figure 3. Scaffolding was set up to raise the FSR to a height where its field-of-view could be covered by the IR detector that was mounted on a 20-foot tower. Figure 4 shows the IR detector mounted on the tower with a view of the containment rings. The FSR is shown in Figure 5 mounted on the scaffold overlooking an oil containment ring.

Figure 2. Test Tank with Oil Containment Rings in Position

Table 1. Setup of Oil Targets During Data Collection

Ring	Dry Run Day	Day 1	Night 1	Day 2	Day 3
1	2 mm Diesel	8 mm Diesel	8 mm Diesel	8 mm Diesel	
2	4 mm Mixed		8 mm Crude	8 mm Crude	8 mm Crude
3	2 mm Waste	3 mm Diesel	3 mm Diesel	3 mm Diesel	3 mm Crude
4	6.25 mm Sundex		3 mm Crude	3 mm Crude	2 mm Crude
5	8 mm Diesel	2 mm Diesel	2 mm Diesel	2 mm Diesel	1 mm Crude
6			2 mm Crude	2 mm Crude	0.5 mm Crude
7		1 mm Diesel	1 mm Diesel	1 mm Diesel	
8			1 mm Crude	1 mm Crude	
9		0.5 mm Diesel	0.5 mm Diesel	0.5 mm Diesel	
10			0.5 mm Crude	0.5 mm Crude	
11					
12		Mixed			

NOTE: Thicknesses indicated are average values; actual thickness varied considerably

Figure 3. Bridge Showing FSR on Scaffold and IR on Tower

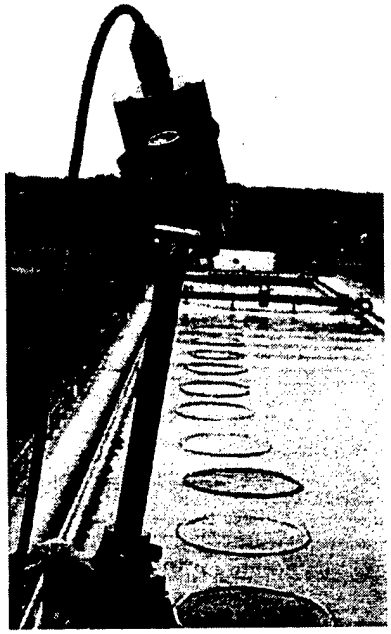

Figure 4. IR Detector Mounted on Tower

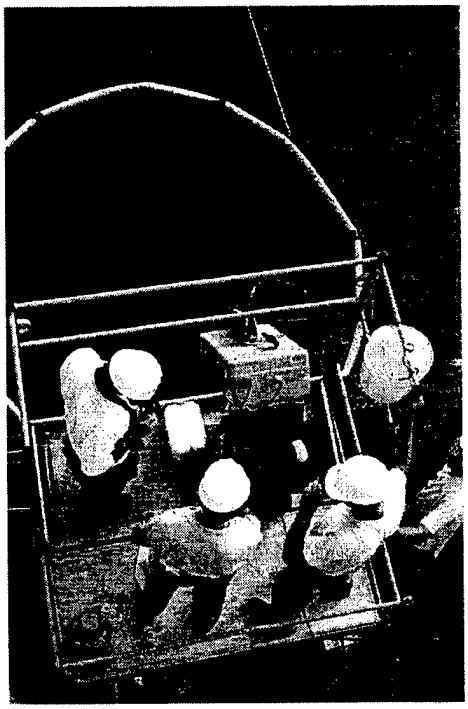

Figure 5. FSR Overlooking Oil Target

2.3 TEST PROCEDURES

During each test period, several tests were performed on each oil slick. Each of these tests consisted of two parts. First the FSR was boresighted with the IR imager. This boresighting was accomplished by using a CO_2 laser mounted on the FSR. This laser was previously aligned with the center of the FSR's field-of-view so that it would be aimed at the same point that the FSR's antenna was looking. At the beginning of each test, the laser was turned on briefly so that it would heat up a small area of the oil. This area would become visible in the IR due to the differential heating. An image of the laser spot would be saved so that the location of the FSR observation could be identified during data processing. One such example is shown in Figure 6.

Figure 6. Oil Target Showing CO_2 Laser Spot

After the area of oil that was heated by the laser had cooled to the ambient temperature of the surrounding oil, the second part of the test was begun. The FSR and the IR took multiple readings of the same spot on the oil slick. At least one IR image was recorded using a thermal dynamic range that included the water temperature and the oil temperature. Other images could be recorded at a lower temperature range in order to increase the resolution of the oil temperature gradients. This procedure was performed at least twice for each oil sample during the test period. At least once during each test period, the bridge was driven from one end of the test tank to the other so that all rings could be viewed in a short period of time. During these runs, IR images were taken of all the rings and the FSR collected continuous data. No collocation was possible during these runs due to the lack of time stamping by the FSR. Near the end of each test period, the fans were turned on for selected rings to create an artificial thickness gradient. The wave generator was used on Day 2 to create two levels of waves and two conditions of harbor chop to test the ability of the instruments under wave conditions. These tank conditions are described in Reference 10.

During the Day 3 test period the FSR was unavailable due to an equipment failure. The IR imager was used alone to take several images of each sample, after which the bridge was driven over all the rings so that images could be taken during a short period of time.

2.4 DATA POST-PROCESSING

The IR imager saves data in proprietary-formatted TIFF files. The files include tags with calibration information including date, time, temperature range, and minimum and maximum temperature of the image. This data had to be read from each image using the IR imager equipment and entered into a spreadsheet for use in determining the temperature value of a pixel.

Once this information was cataloged, the center of the FSR field-of-view was determined by hand for each test. The pixel location of the transient thermal anomaly (induced by the boresighted CO_2 laser pulses) was visually identified and recorded for each thermal IR image. The location was then entered into a spreadsheet. Using this location, software was written to analyze each image and compute the average temperature for a circle with a diameter of 1.07 meters, the calculated field-of-view of the FSR, around the center of the FSR observation.

Each image was then analyzed to determine the average water background temperature that was visible near the corners of the image. For those images that did not have water visible or within the dynamic temperature range used for that image acquisition, the water temperature from other images of the same test ring and time period were used.

The observations of thickness from the FSR were provided by MIT Lincoln Laboratory (Ref. 10) and were correlated with the average temperatures calculated from the IR images that were taken at the same time as the FSR observation. The IR and FSR data were plotted and exponential curves were fit to the data using the Microsoft Excel "Trendline" function. The coefficient of determination, R^2, is also computed to provide a measure of goodness of fit for the relationship between the resulting exponential function and the actual FSR and IR data.

[BLANK]

3. RESULTS

Tests during both daytime and nighttime conditions were performed to determine how the relationship between IR signature and FSR thickness was affected. Testing included four daytime observation periods and one nighttime period. The first day a dry run was conducted to test the equipment and procedures. On the second day, only diesel oil was tested because crude oil was unavailable. That night both crude and diesel oil were tested. Waves and winds from fans were produced during the third day to determine the impact on the FSR readings. The next week crude oil was tested during the day, but the FSR was unavailable due to equipment failure so only IR readings were obtained. During the first two test periods, the sky was partly cloudy. During the night test high winds and rain were observed, and mostly cloudy skies dominated the third day. For the final test day the skies were clear and sunny.

Analysis of the experimental data shows that a relationship between FSR thickness and IR temperature can best be calculated for data collected over a relatively short time period (20-30 min). The environmental effects discussed below are probably responsible for the different relationships found for data collected at different times. In particular the test data collected when the bridge was driven quickly from one end of the test tank to the other exhibited IR temperature signatures that varied with oil type and thickness in a relationship consistent with expected theoretical results.

3.1 ENVIRONMENTAL EFFECTS ON INFRARED SIGNATURE OF OIL

The thermal signature of oil is not based only on its thickness, but on the varied conditions of the local environment and the oil spill. Each of these effects contributes to the detected temperature of the oil in a different way.

When oil is at the same temperature as the surrounding water, it has a different thermal signature because of the difference in emmisivity between water and oil. Seawater has an emmisivity of 0.989, while most oil has an emmisivity of approximately 0.96. This difference translates into an apparent temperature of the oil that is 1.7° C cooler than the surrounding water (Ref. 4). For thinner slicks, less than 0.5 mm, this is the major effect seen in the thermal IR image because the oil is too thin to have an insulating layer between the top of the slick and the water which would allow the oil to achieve different temperatures than the water.

Other variations in temperature are due to the influence of the environment surrounding the slick. These effects are shown in Figure 7. Heating of the oil is caused by solar radiation. Because oil has a specific heat of approximately one-half that of water, it can heat up faster than the surrounding water. Areas that are covered with clouds will heat up more slowly than areas that are not cloud covered.

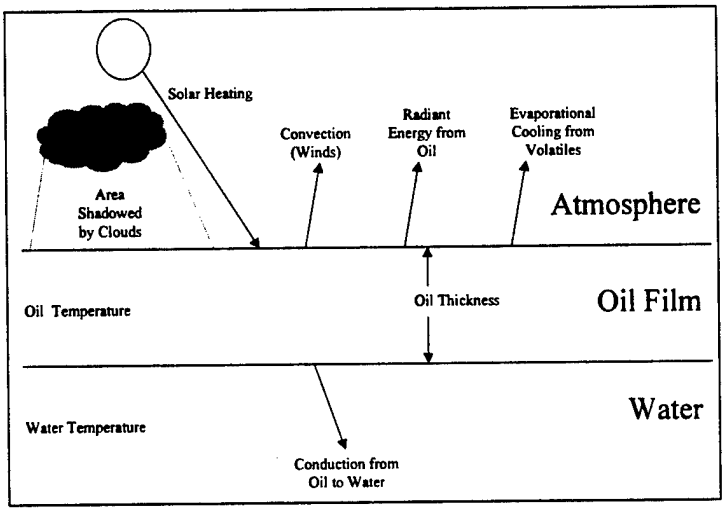

Figure 7. Effects on the Thermal Image of an Oil Slick

Several different processes can cool the oil. Assuming that the water is cooler than the oil (sunny conditions), heat is conducted into the water from the base of the oil slick. The influence of this basal cooling on the top of the slick is dependent on the thickness of the oil. A thicker slick will be more insulated than a thinner slick unless overturning occurs within the slick. Overturning is dependent on the viscosity of the oil, which varies with both oil type and temperature.

From the top of the oil, heat is lost through radiation and convection due to winds. While

the slick is still fresh, Volatile Organic Compounds (VOCs) are also evaporating causing cooling to the top of the slick. These effects on the thermal signature of the slick are difficult to measure. Statistically, one might assume that they act uniformly over the entire area of the slick, allowing associations of oil thickness as a function of observed temperature. However, extensive laboratory testing and modeling of these effects would be required before their actual significance can be assessed.

3.2 INDIVIDUAL TESTS

This section presents results from each test period. Only selected plots of oil slicks are presented here. Appendices A and B contain plots of FSR thickness versus IR temperature difference (oil-water temperature contrast) for all observations. Originally, during data processing it was assumed that relating observations to thermal contrast would serve to mitigate various temporal effects, which occur during data collection. This was later found to have little impact, and subsequent data compilations and presentations preserve the absolute temperatures recorded during the observations. Note that all plots in the main body of this report reference the absolute temperature.

3.2.1 Dry Run Day

Testing on this day was intended to make sure that the equipment was working properly and that the laser boresighting was feasible. Conditions during the testing were sunny with an air temperature of 30° C and a water temperature of 26° C. Various oils were used for testing, including waste oil, Sundex, diesel, and a diesel/Sunex mix. Only the diesel oil had sufficient observations to compute a relationship between thickness and temperature. Figure 8 shows these observations plotted for the 8 mm and 2 mm rings. Only linear fits to these data are shown, due to the limited number of observations.

For this dry run the 8 mm ring readings are cooler than those for the 2 mm ring, which is unusual during daytime conditions. However, 40 minutes elapsed between the two observations which allowed the 2 mm ring to heat up during that time; this could explain the readings obtained. Even though readings for the 8 mm ring are cooler than for the 2 mm ring, the slope of

the readings within the individual rings shows a warming with thickness similar to the exponential relationship seen during observations during subsequent days. The slope of the 8 mm ring data is greater than the slope for the 2 mm ring. This supports the relationships computed on other days.

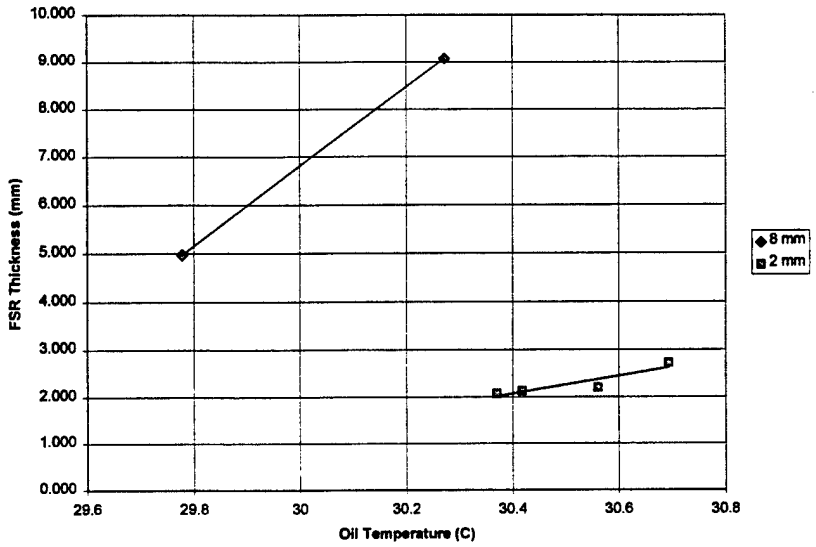

Figure 8. Diesel Oil with Good or Excellent FSR Observations

3.2.2 Day 1

This test period comprised daytime testing of diesel oil. Conditions during this day were partly cloudy with an air temperature of 25° C and a water temperature of 25° to 26° C. Winds averaged 7-8 mph. Results of the FSR thickness versus IR temperature measurements are plotted in Figure 9. The oils between 0.5 and 3 mm exhibit an exponential relationship between thickness and temperature. The coefficient of determination (R^2), a goodness of fit measure, is 0.64. Notice that errors in the FSR thickness estimates for the 0.5 mm and 1.0 mm tests prevent a better fit. More significantly, the 8 mm ring is cooler than the rest of the oil and the relationship between temperature and thickness is not well defined. This could be due to several factors including when the 8 mm ring was poured and how fast the volatiles were evaporating. With thicker oils it may take a longer time for the oil to reach a thermal equilibrium. Also the bridge could have been parked over it prior to the observations, which would cause it to remain cooler than the other samples.

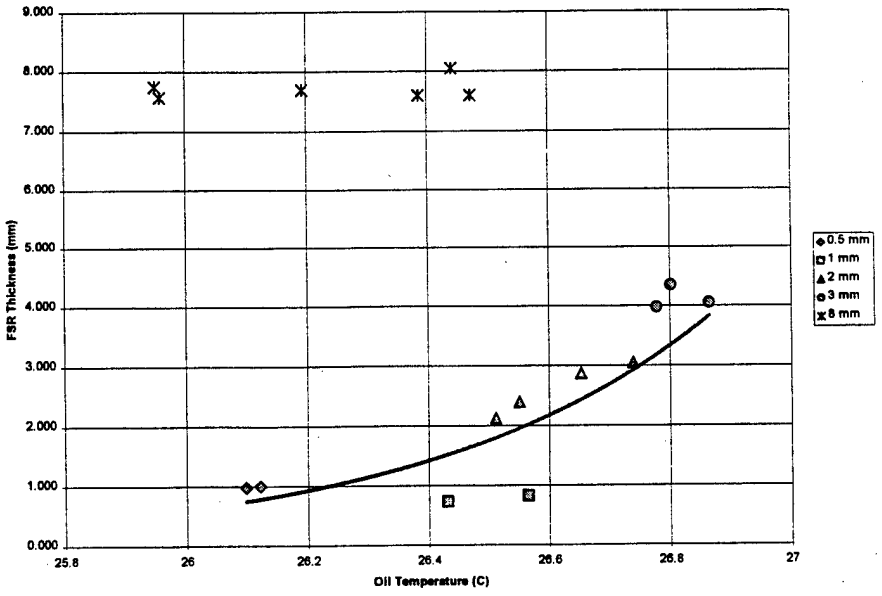

Figure 9. Diesel Oil with Curve Fit to 0.5 – 3 mm Thickness, $R^2 = 0.6414$

At the end of the individual ring testing, the bridge was "flown" over all of the rings and images of each ring were sampled during a short period of time minimizing any effect due to temporally varying environmental factors. The average temperature of the oil within each ring was calculated and plotted against the calculated thickness of each ring in Figure 10 and Figure 11. Thirty minutes elapsed between these "flying" runs, which allowed the environment to affect the temperature. Both plots show a strong fit to an exponential curve. However, in both plots the thinnest oil layer exhibits a warmer temperature than the next thicker layer, possibly because these slicks have a lower total heat capacity and can therefore, during warming, reach thermal equilibrium faster than the thicker oils. The thinner slicks contain less volatiles which could have evaporated off prior to the observation thus allowing them to heat up more because of the reduced cooling due to evaporation. Figure 11 exhibits lower temperatures than Figure 10, which could be due to the cloudy conditions and evaporation of the volatiles. That this relationship is strong during this type of rapid observation shows that time is critical in observing the oil slicks to minimize the impact of the environment on the thermal signature.

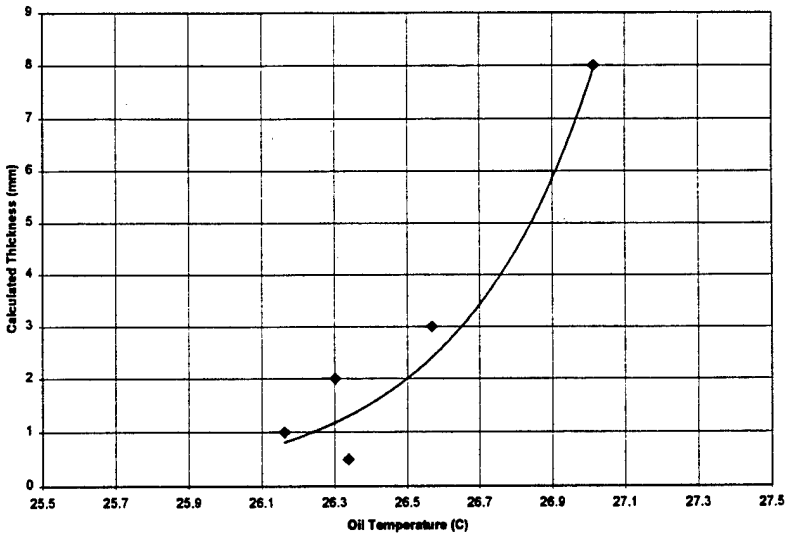

Figure 10. Diesel Oil Fast Run #1, Day 1, $R^2 = 0.7784$

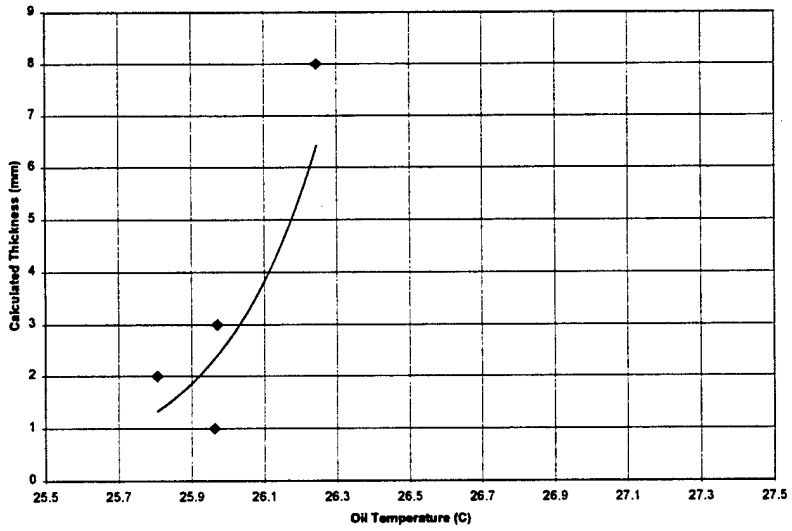

Figure 11. Diesel Oil Fast Run #2, Day 1, $R^2 = 0.5792$

3.2.3 Night 1

Testing of the nighttime effects on the temperature/thickness relationship was performed during only one data collection period. Conditions during the test included rain and moderate winds of approximately 13 mph. Air temperature was 23° C and water temperature was 25° C. Testing during this period also included using the fans in an attempt to pool the oil and create a thickness gradient. Figure 12 and Figure 13 show an exponential curve fit to the observations that did not include the use of fans. This relationship shows that during nighttime or periods of

minimal or no solar heating, the thicker oil appears cooler. This cooling with thickness is expected because thinner oil slicks are transporting more thermal energy from the underlying water. When the fans were turned on, the oil appeared cooler, yet the relationship between the 3 mm and 8 mm diesel oils remains similar in slope to the non-fan observations.

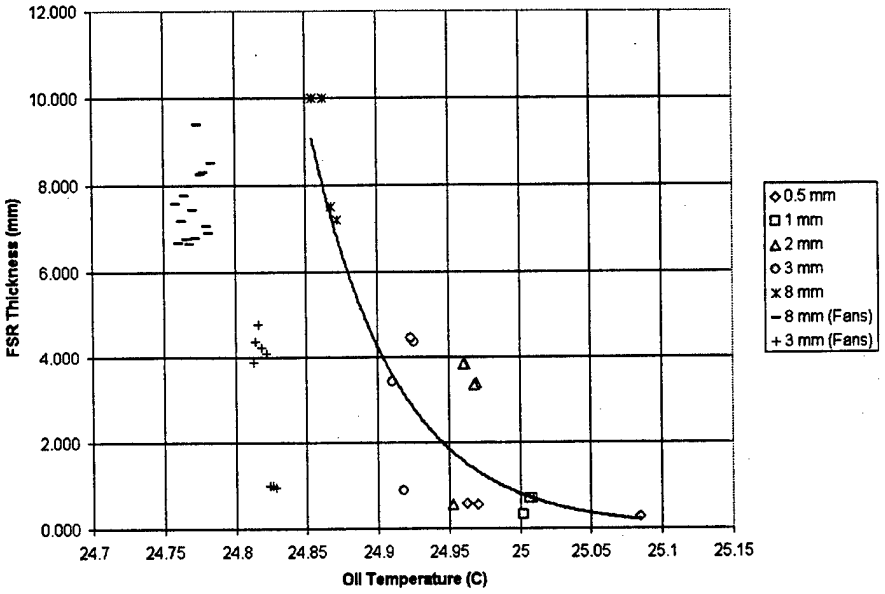

Figure 12. Diesel Oil with Curve Fit to Samples without Fans, $R^2 = 0.6463$

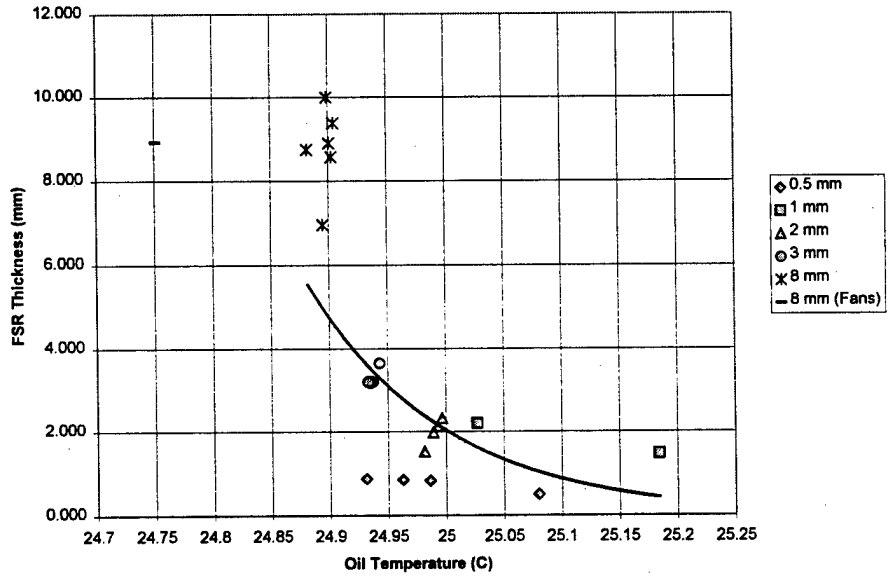

Figure 13. Crude Oil with Curve Fit to Samples without Fans, $R^2 = 0.4412$

A "flying" run was performed on the oils during the nighttime test and images were collected in rapid succession. The average temperature in the rings was plotted against calculated thickness and is shown in Figure 14 and Figure 15. The coefficient of determination (R^2) for these tests is substantially higher (R^2 = 0.85 to 0.90) for these runs than for the earlier tests with the FSR (R^2 = 0.44 to 0.78). This clearly illustrates the significance of temporally varying environmental factors in the conduct of these experiments.

In contrasting these two figures, it can be seen that the crude oil appears cooler than the diesel, which could be due to several factors. The diesel oil is less viscous and under the severe weather conditions experienced during this period, the thinner layers especially could have been subject to more overturning and been more affected by the warmer water than the crude. Also the thicker crude oil could have supported a layer of cooler rainwater on top of it causing the thermal image to include effects of the water.

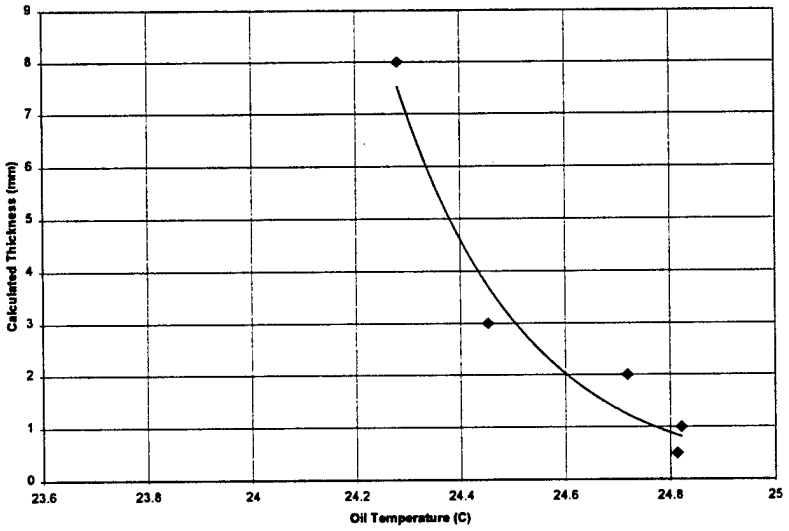

Figure 14. Diesel Oil Fast Run, Night 1, R^2 = 0.8538

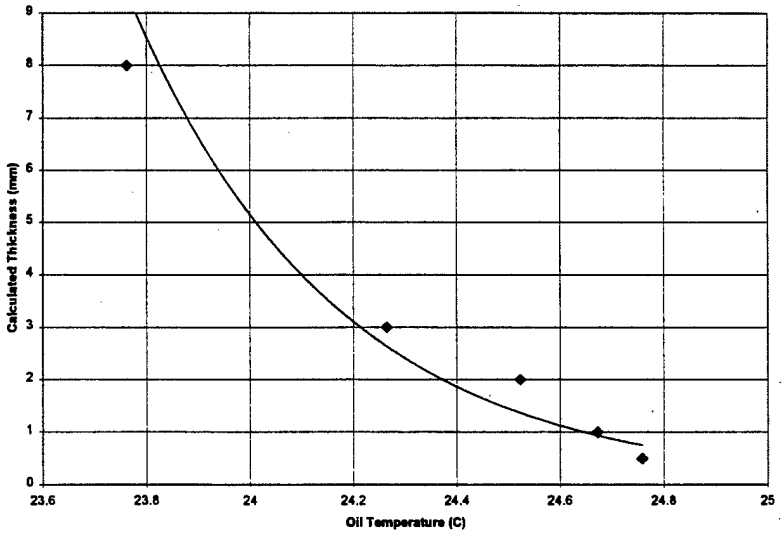

Figure 15. Crude Oil Fast Run, Night 1, $R^2 = 0.9095$

3.2.4 Day 2

Day 2 was used to test the effect of waves and harbor chop on the accuracy of the FSR and IR measurements. Data was collected and plotted, but the amount of data collected is small and the computed relationships are poor. It is difficult to determine the exact cause of the poor relationships. Further testing is recommended to determine the effects of waves.

Prior to the initiation of the waves, another "flying" run was performed and similar relationships to the night test were observed (Figure 16 and Figure 17). In this case the crude oil is similar in temperature to the diesel. The oil still has a profile similar to the nighttime profile. This is not unexpected as the observations were taken around 9:30 am; the sky ranged from partly to mostly cloudy and the wind was generally above 15 knots. The oil was still not exposed to significant solar heating, although the darker crude had warmed slightly more than the diesel.

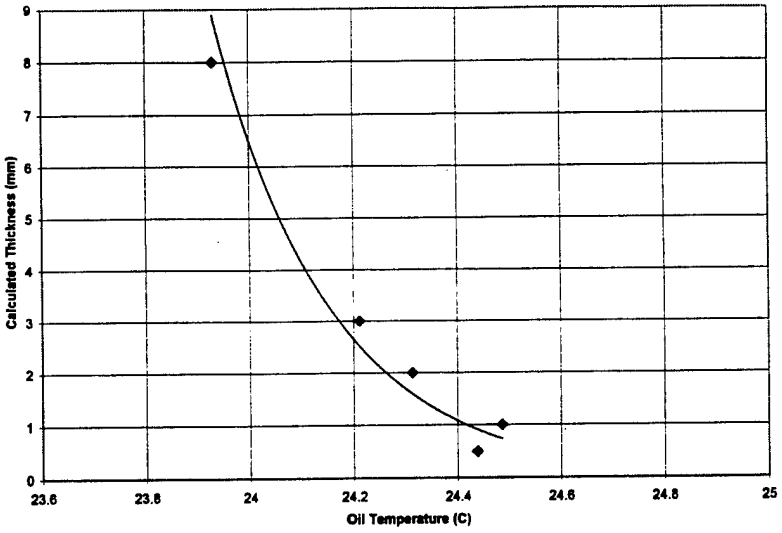

Figure 16. Diesel Oil Fast Run, Day 2, $R^2 = 0.8753$

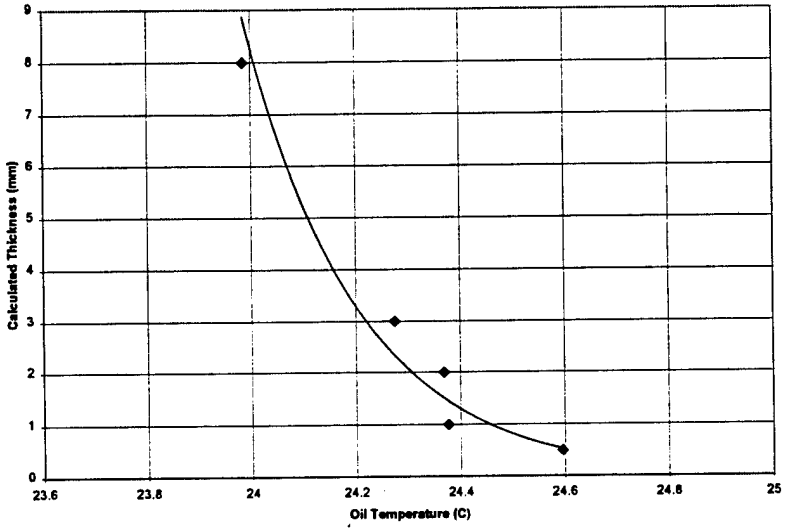

Figure 17. Crude Oil Fast Run, Day 2, $R^2 = 0.9361$

3.2.5 Day 3

During this period the FSR was unavailable due to an equipment failure so only IR images of the crude oil were obtained. Conditions were clear and calm with an air temperature of 21° C and a water temperature of 18° C. After the oil was poured, it was allowed to sit for 1-1/2 hours to achieve a thermal equilibrium. A "flying" run was performed and Figure 18 shows the relationship between calculated average thickness and temperature. This relationship is similar in form to the daytime relationship seen on Day 1 for the diesel oil. There is, however, a much more

dramatic temperature contrast among the samples, demonstrating the potential for the more viscous crude oils to maintain a relatively high thermal gradient.

Individual pool measurements were also performed prior to the "flying" run and an issue with the calibration of the IR detector was discovered. Table 2 shows the average oil temperatures for the 8 mm crude oil slick taken over a 4-minute time period. Different temperature ranges were used to gather information about the water temperature. When the range was reduced from 50° to 10°, the measured temperature of the oil jumped almost 4°C. During most of the testing, the range was set at 2° so this is not an issue with respect to the test data collected, however, it does pose a question about the accuracy and calibration of the IR detector. As stated in Section 2.1, the claimed repeatability of the IR imager is ±0.5°K. Absolute accuracy, which presumably is the governing statistic when changing the instrument dynamic range, is cited as ±2% or ±2°K (no error distribution is referenced). No specification is given for the relative accuracy when switching dynamic range. The owner of the instrument asserts that (accepting the advertised uncertainties) field calibration of the imager is not required. While the observed 4°C shift in observed oil temperature may fall within the published error bounds, such errors may well be limiting to certain operational applications of this and similar instrumentation. Field calibration procedures and tests should be devised to mitigate the uncertainties associated with changes in dynamic range for any future experiments.

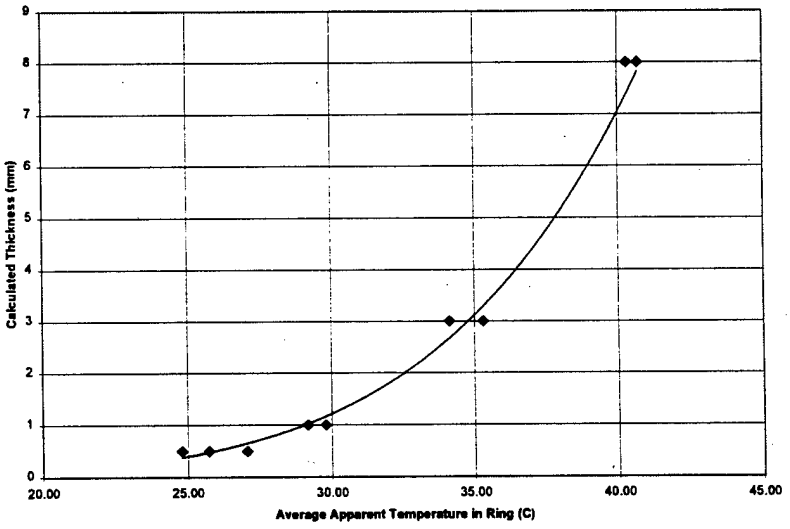

Figure 18. Crude Oil Fast Run, Day 3, $R^2 = 0.9811$

Table 2. Temperature Differences Due to Change in Range of IR Detector

TIME	MINIMUM	MAXIMUM	RANGE	AVERAGE OIL TEMPERATURE
10:53:50	6.5	56.5	50	30.13
10:54:08	6.5	56.5	50	30.72
10:54:47	28.2	38.2	10	34.22
10:55:40	27.9	37.9	10	34.19
10:56:03	27.9	37.9	10	34.70
10:56:22	27.9	37.9	10	34.93
10:56:59	32.7	37.7	5	34.97
10:57:23	32.7	37.7	5	35.43

3.3 THICKNESS MAPS

A key objective in using FSR/IR sensing technology for oil spill monitoring is the estimation of oil thickness. Given thickness as a continuous function of position over some domain, it is clearly straightforward to integrate the thickness over the area to produce an estimate of the volume of oil spilled. Accurate thickness and volume estimates are of major importance in relation to potential recovery operations, mitigation of environmental damage, and assessment of liability.

In principle, the thickness can be estimated whenever there are multiple FSR measurements spanning the full range of oil thicknesses present. Uncertainty in the estimates will be reduced substantially if all the data, both the FSR measurements and the IR imaging, are acquired within a sufficiently short time frame that environmental factors will not have changed the oil temperatures. This probably implies data acquisition for any given thickness/volume estimate within ten to fifteen minutes at most, and preferably less.

During the OHMSETT experiment, data acquisition was generally much slower. As previously discussed, this likely accounts for the weakness of the correlation between FSR thickness estimates and IR temperature for some of the observations. One of the faster series of

combined FSR/IR observations was the (slow) run over the 0.5 - 3 mm diesel oil targets on Day 1. A least-squares fit of the FSR thickness estimates to the IR temperature data for those observations (Fig. 9) produced the exponential function

$$h = 4^{-25\ e2.1369\ t}$$

where h is the thickness of the oil and t is the observed IR temperature. Using this relationship the thermal IR image was classified and contoured according to oil thickness. The result is shown in Figure 19. The same function was then used to classify and contour a second thermal IR observation. This image was acquired approximately 2-1/2 hours later during the fast run for Day 1. This result is shown in Figure 20.

While a somewhat different part of the ring is imaged in the latter acquisition, and the oil concentrations have drifted during the intervening time, it is clear that the order of magnitude for the reported thicknesses is consistent with the 2 mm average thickness originally placed in the ring. Comparison of the two figures would also suggest that the thicknesses reported for the later (fast) run are perhaps a millimeter thicker on average than for the earlier (slow) run. This apparent bias is not unreasonable given the elapsed time between acquisition of the FSR data used for calibration and the thermal IR image itself. As can be seen by reference to the plotted exponential function in Figure 9, it would take a temperature increase of only 0.2^0C in the surface temperature of the diesel oil over the 2-1/2 hour period to cause such a shift. This potential source of error would be substantially mitigated in an operational system designed specifically to ensure prompt and coordinated acquisition of both the FSR and the IR data.

As previously noted, an operational system would also provide volume estimates for an oil spill. This computation is straightforward, given the thickness maps; it simply requires the integration of thickness over the imaged area. For a controlled spill, where the total volume of oil being released is known, the volume computation would provide an effective check on the accuracy of the thickness mapping technique. Unfortunately, given the viewing constraints during the experiment at OHMSETT, the thermal IR optics were inadequate to view the entirety of any single containment boom. A valid volume comparison was thus precluded.

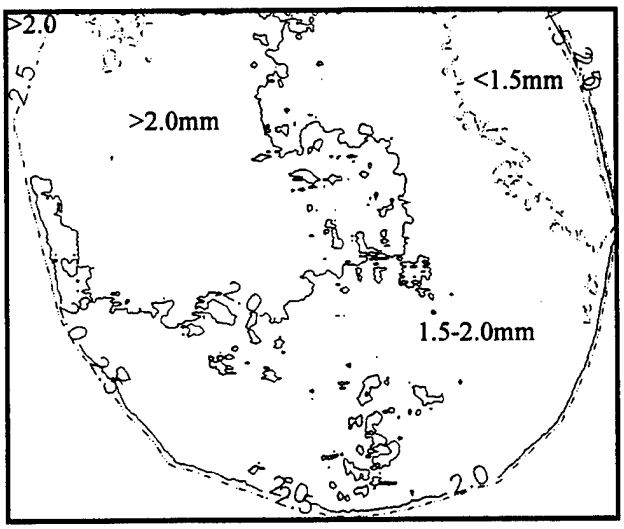

Figure 19. 2mm Diesel Oil Image From Day 1 During Slow Runs Computed From Figure 9 Relationship

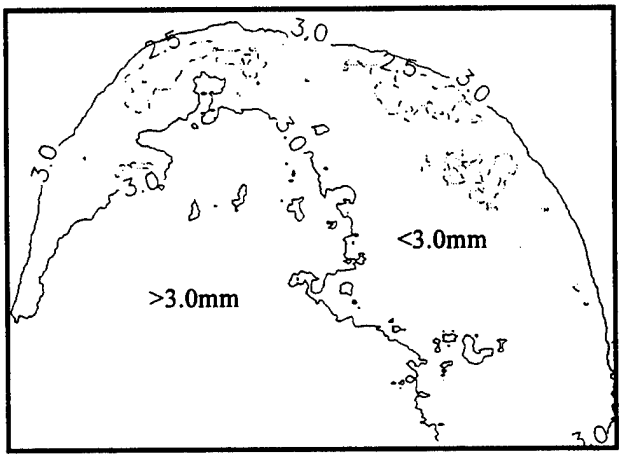

Figure 20. 2mm Diesel Oil Image From Day 1 During Fast Runs Computed From Figure 9 Relationship

4. FUTURE WORK

4.1 FUTURE EXPERIMENTS

In principle, an integrated FSR/IR system could now be designed for operational use in oil slick monitoring from a helicopter. There are, however, several factors involving the scientific basis for the monitoring technique, as well as related system design and procedural issues, which indicate the desirability of further study prior to system design. Some of these involve further testing with experiments related to the OHMSETT exercise reported herein, and this is the subject of the first recommendation below. Other issues relate more to the feasibility of operating such a system in a helicopter environment. One might progress directly to an airborne test, but it would likely be more practical to take a slightly phased approach to that objective. A second test recommendation addressing this subject is also presented below.

Regarding the scientific basis for an FSR/IR system, much has been written on the use of thermal IR for oil slick detection and monitoring. However, the thermal response is highly sensitive to a variety of temporally varying factors, including weather, sea state, and oil chemistry and physical properties. Admittedly, the FSR/IR monitoring concept is designed to mitigate a need for comprehensive understanding of many of these factors. Nevertheless, it may be difficult to design a monitoring system properly unless the operational constraints dictated by such factors are adequately understood. Specifically, the thermal transfer rates induced by wind, rain, and wave motion may place significant limitations on the operational use of such a system. Depending upon the development cost, it may be feasible to design a system and use it operationally when possible, or it may be prudent to understand better the likely operational limitations of the system prior to development. This would suggest that a tradeoff between estimated development costs and the cost of more extensive pre-development testing would be in order.

If a more comprehensive understanding of such environmental and temporal factors were desired, we would recommend a relatively straightforward test series involving just the thermal IR imaging radiometer. A possible test scenario would be as follows:

The IR sensor will be used to monitor four sample (contained) oil spills over a period of several days. Preferred thicknesses for these spills are 0.5 mm, 1 mm, 3 mm, and 8 mm set up as shown in Figure 23, although the actual thicknesses should be determined prior to the experiment. A wide-angle lens should be acquired for the IR imager so that all four rings will appear in a single image and the image recording should be automated. The existing instrumentation at OHMSETT would be used to collect all other environmental data with the addition of a pyrheliometer or similar instrument to measure incoming solar radiation. During the first 48 to 72 hours, all instruments (including the IR imager) should collect data at 10-minute intervals continuously throughout the entire period. After this period of collection, the wave generator should be turned on for a 2-hour period during daytime and another 2-hour period at night to examine the effects of waves on the thermal signature. Data collection for the wave periods should be at 5-minute intervals or less.

This experiment would have the advantage of providing a comprehensive data set to characterize most of the significant temporal factors in one well-controlled study. The most important issues to be resolved from such a study would be a good understanding of the characteristic times associated with the several pertinent heat transfer mechanisms which affect the interpretability of the thermal IR data. Significantly, however, this experiment would also allow the recognition of related operational constraints which might impact the usability of the system, and hence the cost-benefit of development.

A second recommended experiment includes the use of the FSR and is designed to address certain hardware and software issues prior to any attempt to configure the system for actual testing in a helicopter. A scenario for this test series follows:

The FSR and IR radiometer, along with all associated power supplies, calibration equipment, computers, and data archive peripherals, should be set up and tested to demonstrate systems compatibility, reliability, and throughput capability. Significant new software would be required to allow near real time data processing and product generation (including rapid thickness estimates from the FSR, correlation with the thermal IR imagery, thickness map generation, and oil spill volume estimation). Operational requirements, with specific reference to power requirements, physical space, required manpower, communications, and environmental considerations (e.g., vibration, acoustic and electronic noise, and wind levels in an open helicopter cabin) must be thoroughly evaluated prior to any attempt to mount an actual airborne test. It would be appropriate to conduct a field test with such an integrated system at OHMSETT. Unlike the procedures

employed in the September 1996 test, however, the emphasis should be on fast data acquisition. Several fast runs over a series of containment rings should be conducted, similar to the "flying" runs reported earlier in this report, but now incorporating fully coordinated FSR data acquisition and near real time data reduction. This would verify that the integrated system was ready for testing in an operational airborne setting and could produce the desired oil thickness maps and volume estimates in a timely manner. Upon successful completion of these demonstrations, the systems should be evaluated in a helicopter on the ground to identify any unforeseen operational issues prior to design of an actual airborne test.

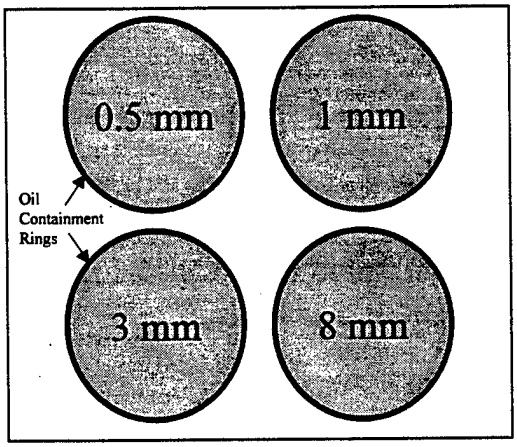

Figure 21. Setup of Oil Targets for Infrared-Only Experiment

4.2 AIRCRAFT ISSUES

This section identifies and describes the aircraft-related issues associated with installation and operation of an FSR/IR instrument on a helicopter. The considerations cited are derived from discussions held between TASC and MIT Lincoln Laboratory personnel as part of this study. Issues that need to be addressed prior to the actual mounting of the instrument in a U.S. Coast Guard helicopter can be divided into three areas: airframe mechanical, airframe electrical and FSR/IR system considerations.

4.2.1 Airframe Mechanical Issues

The majority of the airframe mechanical issues associated with installation and operation of an FSR/IR sensing system must be addressed by a certified aircraft mechanic knowledgeable with regard to the intended helicopter platform. It is anticipated that the primary issues potentially impacting flight worthiness are the impacts on weight and balance of the instrument

package and the operating personnel. Estimated total weight for the combined sensors is approximately 60 pounds, including two laptop computers and all necessary cabling. Two nominal adult male operators would add another 340 pounds. Allowing for other monitoring and communication equipment as well as an inverter to supply the 110 VAC (60Hz) electrical power necessary for the equipment, the total operational load would likely be on the order of 450 pounds. With respect to balance, most of this load would be centered at a station coincident with the cabin door.

Equipment mounting techniques must be researched, as the standard sensor and computer equipment used presently has not been designed for a high vibration environment. Shock mounting will likely be required, and may have an impact on helicopter operation, especially since the system must be mounted proximate to the door for adequate viewing. This may also impact safety, as egress could be compromised, depending upon the mounting/stabilization techniques actually implemented. In any case, the sensor mounts must allow easy and prompt adjustment of the sensor lines-of-sight in both azimuth and depression angle. The mounting system should be adequate to allow a clear field-of-view at azimuths ranging (approximately) from 40 degrees ahead to 40 degrees behind the beam and at depression angles ranging (approximately) from 20 to 60 degrees below the horizon.

Operationally, there must be a good voice communication link between the sensor team and the pilot, in order to facilitate target acquisition and station keeping during data acquisitions. A video link from the IR sensor to a display in the cockpit would facilitate this function, if an appropriate location for a small monitor can be identified.

While the above considerations are adequate for airborne testing of an FSR/IR sensor system (see also the discussion in Section 4.2.3), other capabilities may come into play for an operational system. Perhaps most important is the ability to determine the exact location being imaged. This implies knowledge of the helicopter location, including altitude above the sea surface, and the absolute orientation of the sensor lines-of-sight. Some GPS-based navigation systems have the capability of providing the former with sufficient accuracy, although radar altimeter data might be required to determine altitude with sufficient accuracy for lower altitude

operations. Aircraft inertial systems do not, however, generally provide attitude data adequate to specify sensor lines-of-sight with the necessary accuracy. In addition, it is often a difficult integration task to gain access to aircraft attitude and navigation system data. A more straightforward approach to these geo-location needs is to use a dedicated GPS/IMU system. The IMU is mounted right on the sensor package so that sensor attitude references are totally independent of the aircraft attitude. Such systems have been developed by several commercial vendors, and the weight penalties and power requirements for the GPS/IMU hardware should not be major factors in system integration. The advantage of this approach is that each image acquired may be immediately geo-referenced. Availability of this information also enables auto-mosaicking of the imagery and computation of thickness maps over areas exceeding the field-of-view for an individual IR image frame. This may be particularly important in determining the scale and severity of larger oil spills.

While weight and power requirements for the navigation and attitude sensing equipment are not particularly great, their use would impact the overall hardware requirements and add considerable complexity to the system integration task. Perhaps most significant is the issue of event timing. Given the helicopter motion, the sensor attitude must be very accurately referenced to the times of data acquisition. To accomplish this at least one of the currently required laptop computers would have to be swapped with a mid-sized or larger personal computer (PC). There would be some increase in total weight (perhaps 30 pounds, including PC, cables, GPS receiver and antenna, and increased power inverter capacity to handle the additional hardware). There are also issues associated with mounting the GPS antenna. Unobstructed GPS satellite visibility is a firm requirement, but in addition there may be significant multi-path problems arising from the helicopter rotor for antennas in many locations. Identifying a satisfactory location may in itself require significant effort and testing. Standard GPS positional accuracy is on the order of 15-30 meters under most conditions, given the availability of military GPS codes. If more accurate geo-location is required, either differential or kinematic GPS techniques may be employed, but both of these also require a communications link with a surveyed GPS ground station. This in turn would dictate the need for a communications antenna and receiver, which are integrated with the sensor package. It should be noted that the system described here does not comprise an off-the-

shelf system. Both the hardware and the software integration tasks would require a significant effort and involve substantial testing, particularly if the position/attitude sensing capabilities were required.

4.2.2 Airframe Electrical Issues

An appropriately certified aircraft mechanic will be required to assess fully the electrical issues associated with operating an integrated FSR/IR system on board a helicopter. The first issue is, of course, the provision of adequate and sufficiently regulated power. The basic system as operated at OHMSETT requires approximately 100 watts at 110 VAC / 60Hz. The use of a larger computer, cockpit monitor, and the associated GPS/IMU hardware required for precision navigation and attitude information would likely require an additional 300 watts. Power conditioning hardware, if needed to ensure reliable operation of this hardware could also increase the total weight of the package. The tolerance of the hardware to voltage anomalies and the quality of the on board power supply are both issues for further study.

Unless appropriate power sources are already available in the helicopter cabin, these requirements would necessitate installation of a new power feed, preferably using a spare breaker on the avionics bus to minimize impact of the installation. A separate power cutoff switch would also be needed in the cabin, giving both the pilot and the sensor operators independent capability to cut power in an emergency. If supply of power becomes a difficult matter, it may be possible to perform initial tests under battery power (at some additional weight penalty, and not including any of the precision navigation/attitude sensing hardware).

4.2.3 FSR/IR System Issues

Electronic noise is another potentially significant issue, especially with regard to the FSR. While neither sensor is an active device, there is at least the potential for interference between the helicopter avionics systems and the sensor package, or vice versa. A properly certified avionics technician will be needed to review the planned installation. The most significant concern is for any spurious noise in the 26-40 GHz range, that part of the microwave detected by the FSR. This issue is critical and should be assessed before any other effort is undertaken. Sufficient time must

also be allowed to test for any other noise issues and to resolve such difficulties prior to flight testing. Any shielding and grounding requirements which evolve from such testing are not likely to impact significantly the total weight or design of the system.

Regarding testing of the microwave noise issue, the FSR should initially be operated near the helicopter, but on the ground, as all electronic and avionics systems are turned on (sequentially). This will assist in identifying any specific noise sources, as well as affording the helicopter crew an opportunity to note any adverse impacts from the FSR/IR electronics. If successful, a subsequent ground test should be run using helicopter-supplied electrical power for the sensor package. The impact of any electronic noise on the FSR will be limited, as necessary, by using a sealed EMI case, isolating the power supply and running the amplifiers from batteries.

In addition to concerns over EMI, there are also some geometric considerations in the use of this instrumentation. First, the boresighting of the IR radiometer to the FSR, which was addressed through use of the CO_2 laser during the OHMSETT experiment, will be handled differently for airborne operations. For these flights the two sensors will be attached to a common mount and pre-aligned in the laboratory. Apart from co-alignment of the two sensors, the user must also be able to determine the geographic location being sensed. This requires knowledge of the sensor position (three-dimensionally) and attitude, as previously discussed in Section 4.2.1. While the approach outlined there is accurate and robust, and may be preferred for operational use of the sensors, there may be simpler, less expensive solutions which can be used at least for testing purposes.

If the helicopter is flown slowly and is held at a near zero degree roll attitude during data acquisition, the sensed location may be approximated as the helicopter location. The errors in this position estimate are principally the error in estimating the helicopter location at the estimated time of image acquisition, the motion of the helicopter between the estimated and actual time of exposure, and the horizontal range from the helicopter to the sensed target, where the last may be expressed as:

$$R = h \tan (90 - \theta)$$

R being the horizontal range, h the helicopter altitude above mean sea level (MSL), and θ the sensor depression angle below local horizontal. Assuming a typical depression angle of 60 degrees, R would range from about 90 to 350 meters for acquisition altitudes of 500 - 2,000 feet (150 - 610 meters) MSL. Using typical GPS navigation, constraining groundspeeds to less than 50 knots (25 m/s), and allowing up to a six-second uncertainty in manually referencing the time of sensor exposure to helicopter location, the horizontal range would be the dominant source of position error. These errors could be further reduced by referencing the height above sea surface and the helicopter heading at the time of data acquisition.

With an FSR/IR sensor installation alone, thickness maps and oil spill volume estimates could be produced quickly from individual IR image frames (using thickness calibration data derived from multiple frames acquired over a short period of time). However, multiple frames could not be adequately geo-referenced to allow mosaicking of those frames. For this reason, mapping of an entire spill and computation of its volume would not be possible without the additional geo-referencing hardware and associated software previously discussed in Section 4.2.1.

4.2.4 Additional Issues

Other issues which must be addressed prior to flight testing include:

- Defining safe calibration procedures for the FSR, for which liquid nitrogen is currently used
- Calibration of the thermal IR radiometer, especially to eliminate biases associated with operational changes in the dynamic range
- Coordination of communication procedures between helicopter crew and sensor operators
- Development of all necessary software for integrated test hardware
- Capture of all necessary position, altitude, attitude, and frame time data for observations made with experimental configuration (no precision navigation and attitude instrumentation mounted on the sensor system)
- Documentation of and training for all operational considerations including installation procedures, space allocation, safety considerations, emergency procedures, and lighting and other environmental issues (including wind in the cabin)

It should be recognized that the above comprise a preliminary list of issues for consideration in planning flight tests of an FSR/IR system. It is expected that additional concerns will arise as the test system is developed, the helicopter platform is evaluated, and test plans are made.

[BLANK]

5. CONCLUSIONS AND RECOMMENDATIONS

5.1 CONCLUSIONS

Based on thermal infrared (IR) imagery and frequency scanning radiometer (FSR) data collected at the OHMSETT facility in September 1996, a quantitative relationship between oil slick thickness and infrared temperature of the oil can probably be determined under many circumstances and used to generate thickness maps of the oil. While the IR imagery provides spatial coverage and a measure of relative oil thickness in this remote sensing concept, the FSR data allows calibration of the IR imagery with absolute thickness determinations. The robustness of the thickness/temperature relationship is dependent on various local environmental factors which affect the surface temperature of the oil. Because these factors are temporally varying, the accuracy may also be impacted by data collection procedures, especially if there are significant delays in data acquisition. Since the OHMSETT experiment was not designed to emphasize the speed of data collection, and not all environmental factors were adequately monitored, the test can best be characterized as a significant, but limited, success. Additional observations and further testing are needed to determine adequate operational guidelines and constraints, specifically addressing these environmental factors for various types of oil, prior to fielding an airborne FSR/IR instrument.

During the OHMSETT experiment, infrared imagery and FSR thickness data were collected from several oil containment rings, each with a different thickness or type of oil. These data were collected sequentially, over a period of time, allowing for multiple FSR readings from each individual ring. Observation time for the full series of rings was typically in excess of thirty minutes. The full series (all rings) was then repeated during a much shorter period of time (typically a matter of three to four minutes). The FSR and IR data were combined for the (slower) individual ring observations, and the plots of this data show a weak relationship between FSR-determined thickness and IR temperature. During the rapid data collection periods, data from the FSR was not boresighted with the IR radiometer. Instead of correlating temperature with FSR-derived thicknesses, the average thicknesses (based on OHMSET records of the

volume of oil dispersed in each ring) were used. This resulted in much more well-defined relationships between oil thickness and IR temperature. We believe that the differences between the two techniques are due to temporally varying environmental factors and their effect on the temperature of the oil during the course of the observations. The half hour or so required to complete the slower data collection series is clearly sufficient for changes in solar insolation, wind velocity, and both radiative and evaporative cooling (to mention just a few of the more significant heat transfer mechanisms) to perturb the temperature of the oil slick surfaces. The rapid observation series substantially limit the time over which these temporal influences can affect the thermal signatures, resulting in much stronger correlation between the oil thickness and the observed thermal IR data.

5.2 RECOMMENDATIONS

Further testing is recommended prior to implementation of an airborne instrument. First, we recommend repeating elements of the OHMSETT FSR/IR integration test, but with some very significant procedural changes. For this test, the emphasis should be on observations of different thicknesses of oil, taken in rapid succession to prevent undesired variations due to environmental heating or cooling. This is important to establish the robustness of the correction between FSR-determined oil thickness and the temperatures detected by the thermal imager. By emphasizing the speed of data acquisition, the test will more nearly approximate a typical operational scenario. In an airborne remote sensing application, the FSR would be used to calibrate a slick spanning a large area, possibly imaged as a single frame, but more likely covered by several rapidly acquired frames of imagery. The entire suite of imagery would be acquired within seconds, or perhaps a few minutes. Data acquisition in this mode would certainly be much faster than the time constants associated with the various environmental factors which alter the surface temperature and tend to confound the FSR/IR data correlation.

Techniques for field calibration of the infrared radiometer should also be evaluated. Data collected during the OHMSETT experiment suggest that there may be significant temperature biases encountered when switching the dynamic scale of the IR radiometer. While further testing is needed, there is no data to suggest that simply altering the range while leaving the scale setting

fixed will produce temperature errors. This understanding should be evaluated by observing essentially isothermal targets at various ranges and at all scale settings. Initial range settings should be repeated for all scales to identify possible variation in the target temperature as well as instrument repeatability. Repeat testing could be used to determine whether biases associated with different scales are static, random, or environmentally dependent. Should these biases prove to be non-deterministic, appropriate operational constraints (e.g., using a fixed scale for any one observation series) can be defined to ensure the accuracy of at least the relative temperatures observed.

In addition, testing should include observations to quantify the effects of the various dynamic environmental factors on the thermal signature of characteristic oil types. We recommend using the IR imager to obtain an essentially continuous record of the thermal signature for several separate rings, each with a different thickness of oil. By using somewhat smaller containment rings, all thickness could be imaged simultaneously. Each simulated spill would by design be subject to the same sequence of environmental heating and cooling, greatly simplifying the data analysis problem. The results would yield a vastly improved understanding of the relative roles played by these environmental factors as they impact the thermal signature of the various oil types. Any environmental conditions and constraints which could impact the successful use of an integrated, airborne FSR/IR monitoring system could then be identified and used to help define operational techniques and limitations.

5.3 SUMMARY

The use of an FSR to calibrate the relationship between oil thickness and oil slick surface temperature appears to have merit, based on the results of this experiment. Before an operational system could be fielded, however, there must be an improved understanding of the several environmental factors which affect the heating and cooling of the oil slicks. Operational scenarios for the use of an integrated airborne monitoring system must be developed with appropriate recognition of the characteristic times associated with the thermodynamic aspects of these environmental factors.

[BLANK]

REFERENCES

1. Murphy, T.J. and O.B. McMahon, *Design and Test of a Multichannel Ka-Band Radiometer for Thickness Measurement of Oil Films on Water*, Lincoln Laboratory, Massachusetts Institute of Technology, January 1997.
2. Murphy, T.J., O.B. McMahon and G.L. Hover, Test Tank Evaluation of a Frequency-Scanning, Microwave Radiometer to Estimate Oil Slick Thickness and Physical Properties, U.S. Coast Guard Report No. CG-D-18-96, April 1996.
3. Hover, G.L., T.J. Murphy, E.R. Brown, G.G. Hogan and O.B. McMahon, Design, Construction, Test and Evaluation of a Frequency-Scanning Radiometer for Measuring Oil Slick Thickness, U.S. Coast Guard Report No. CG-D-29-94, June 1994.
4. Salisbury, J.W., D.M. D'Aria and F.F. Sabins, Jr., Thermal Infrared Remote Sensing of Crude Oil Slicks, *Remote Sens. Environ*, **45:225-231**, 1993.
5. Daniels, G.M., and G.L. Hover, The Detection of Oil Slicks at Night With Airborne Infrared Imagers, U.S. Coast Guard Report No. CG-D-30-94, December 1994.
6. Hover, G.L. and J.V. Plourde, Evaluation of Infrared Sensors for Oil Spill Response Operations, U.S. Coast Guard Report No. CG-D-18-95, June 1995.
7. Goodman, R., Overview and Future Trends in Oil Spill Remote Sensing, *Spill Science & Technology Bulletin*, **1-1:11-21**, 1994.
8. Goodman, R.H., Simple Remote Sensing System for the Detection of Oil on Water, Environmental Studies Research Funds, Report No. 098, Ottawa, 1988.
9. *http://www.inframetrics.com/products/700/index.htm*
10. Murphy, T.J. and O.B. McMahon, Quick-look Analysis Results of Data Collected at OHMSETT During September 1996 Using a Ka-Band Radiometer to Estimate Oil Thickness, Lincoln Laboratory, Massachusetts Institute of Technology, January 1997.

[BLANK]

APPENDIX A: COMBINED PLOTS OF SIMILAR OILS FOR DIFFERENT ENVIRONMENTAL CONDITIONS

This appendix contains plots of FSR-determined oil thickness versus IR temperature difference for all thicknesses of the same oil type which were measured during the same test period. As noted in Section 3.2 the abscissa on the plots in this appendix is temperature difference. This is the value of the observed oil temperature less the temperature of the adjacent water surface at the time of IR image acquisition, expressed in degrees Celsius. A key showing the nominal thickness associated with each observation is provided, except where all data points are for a single ring (in which case the nominal thickness is cited in the figure caption). Linear trendlines are provided on most figures to show the relationship of various observations within the same ring. Each set of measurements is plotted twice. The first plot contains all observations and the second plot contains only observations that have FSR thicknesses that were characterized as "Good" or "Excellent" by MIT/LL. The plots are temporally ordered according to test series.

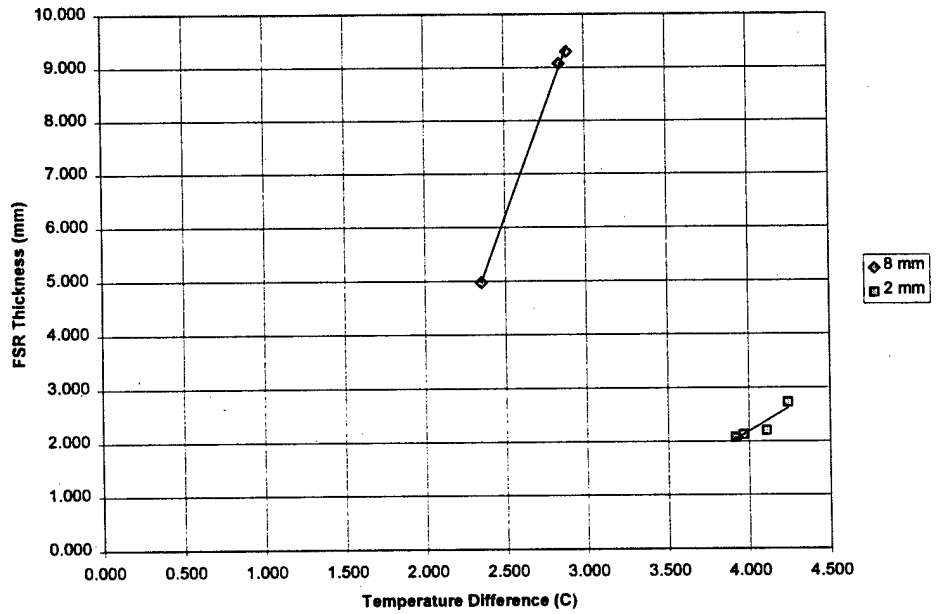

Figure A-1. All Diesel Oils for Dry Run (10 September 1996)

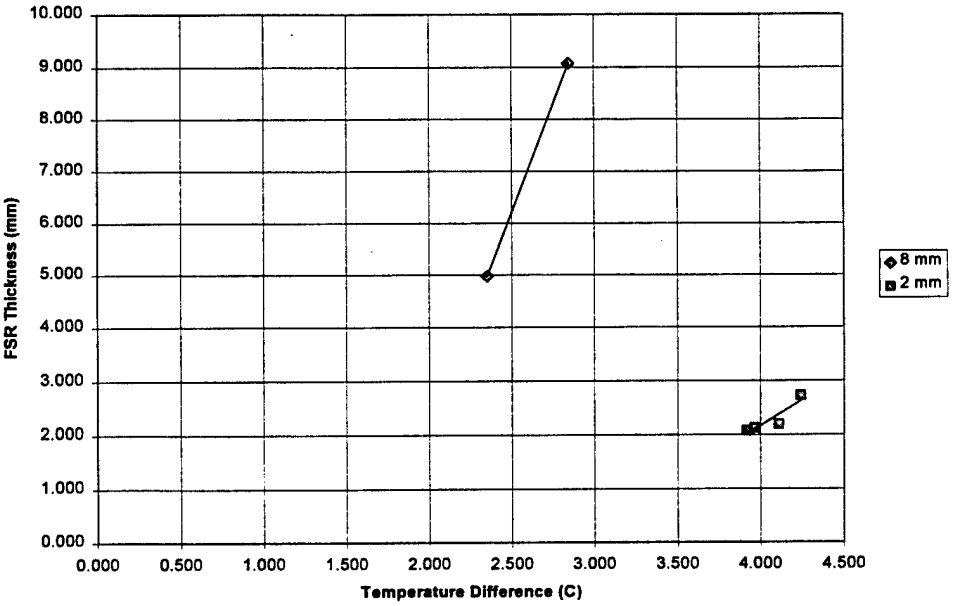

Figure A-2. Diesel Oils for Dry Run with "Good" or "Excellent" FSR Readings (10 September 1996)

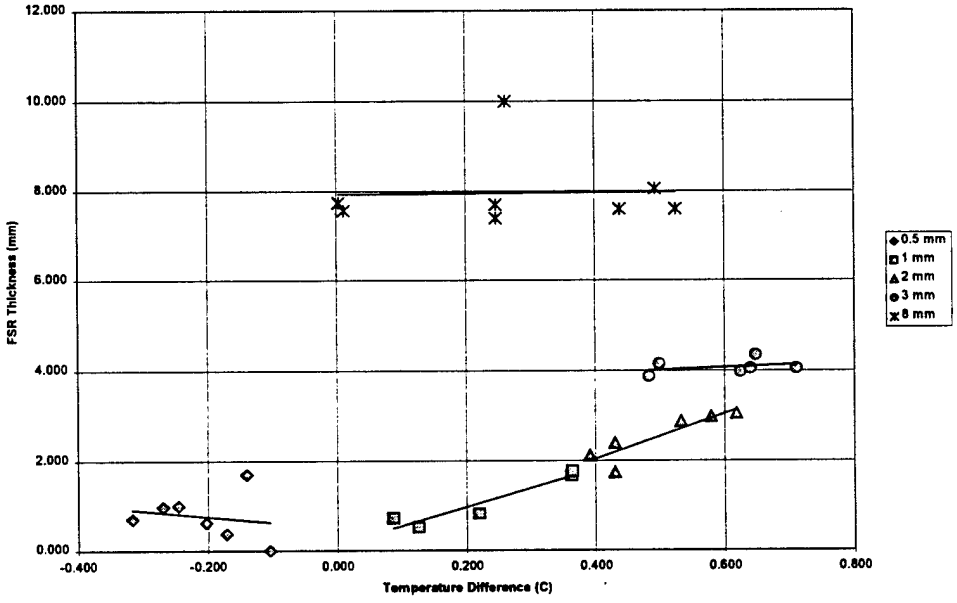

Figure A-3. All Diesel Oils for Day 1 (11 September 1996)

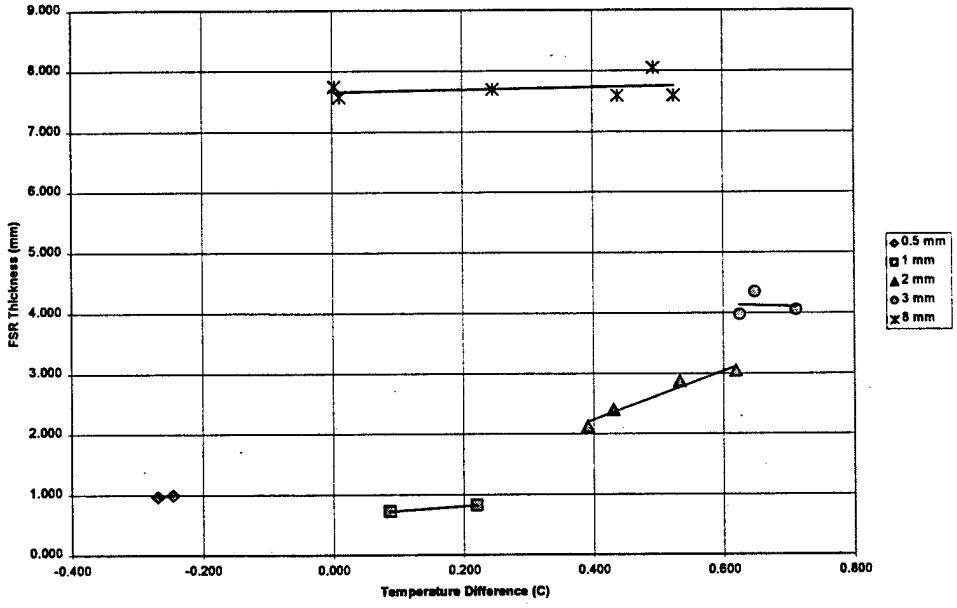

Figure A-4. Diesel Oils for Day 1 with "Good" or "Excellent" FSR Readings (11 September 1996)

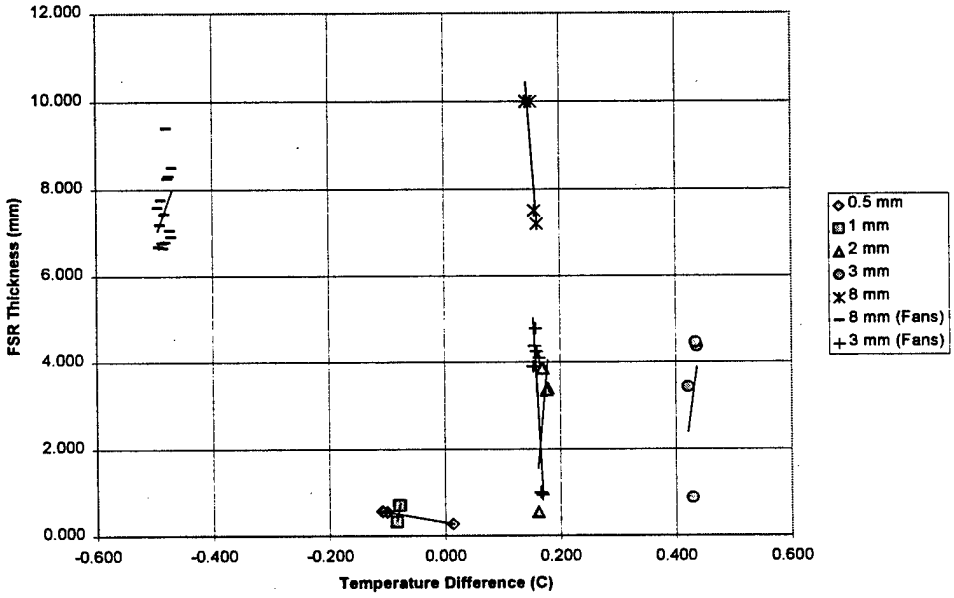

Figure A-5. All Diesel Oils for Night 1 (12 September 1996)

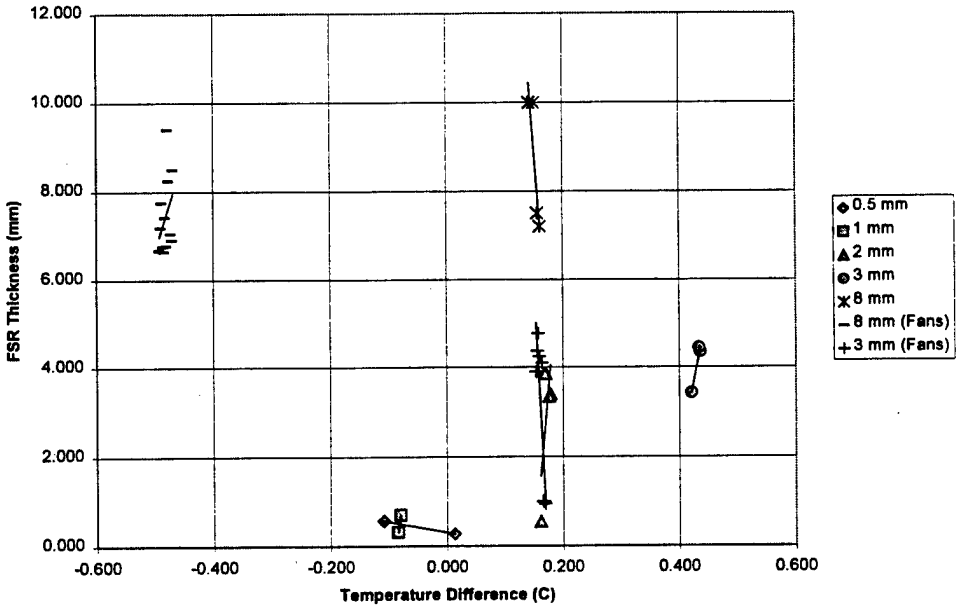

Figure A-6. Diesel Oils for Night 1 with "Good" or "Excellent" FSR Readings (12 September 1996)

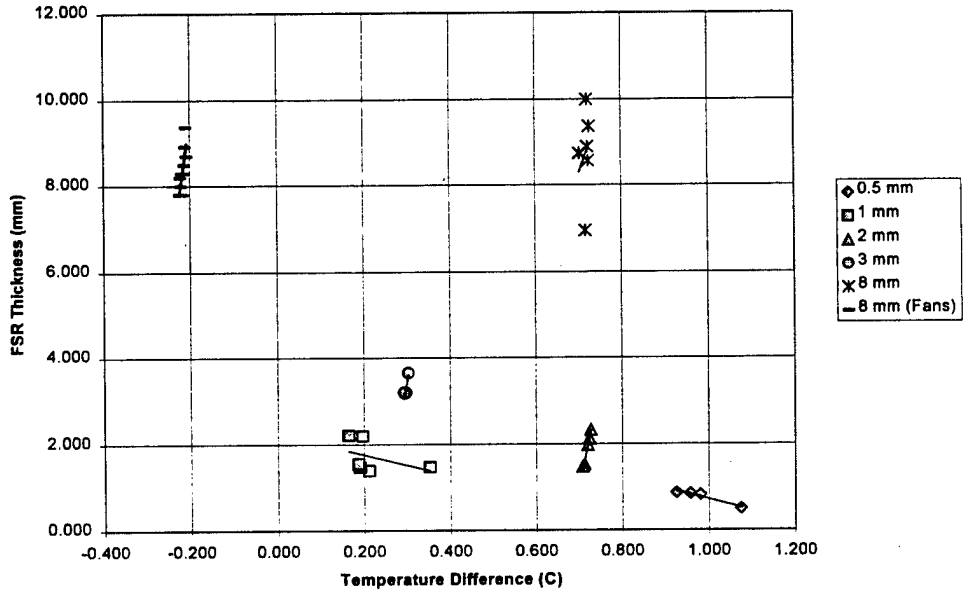

Figure A-7. All Crude Oils for Night 1 (12 September 1996)

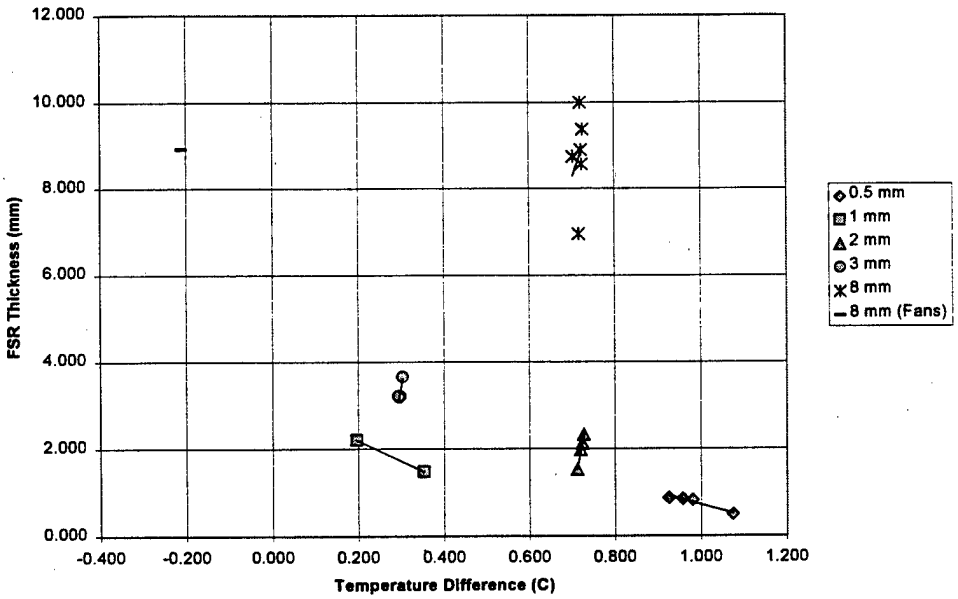

Figure A-8. Crude Oils for Night 1 with "Good" or "Excellent" FSR Readings (12 September 1996)

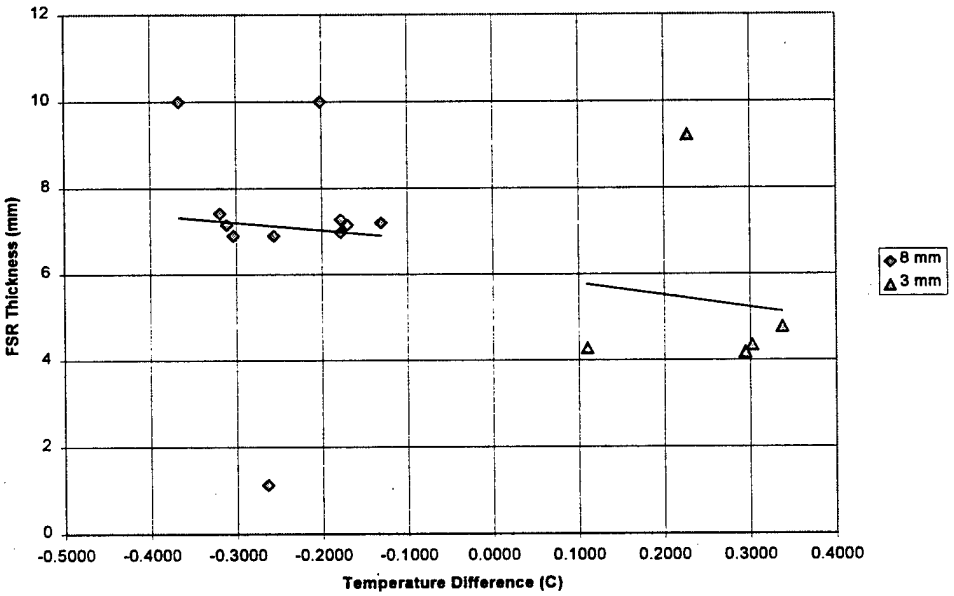

Figure A-9. All Diesel Oils During Wave Conditions for Day 2 (12 September 1996)

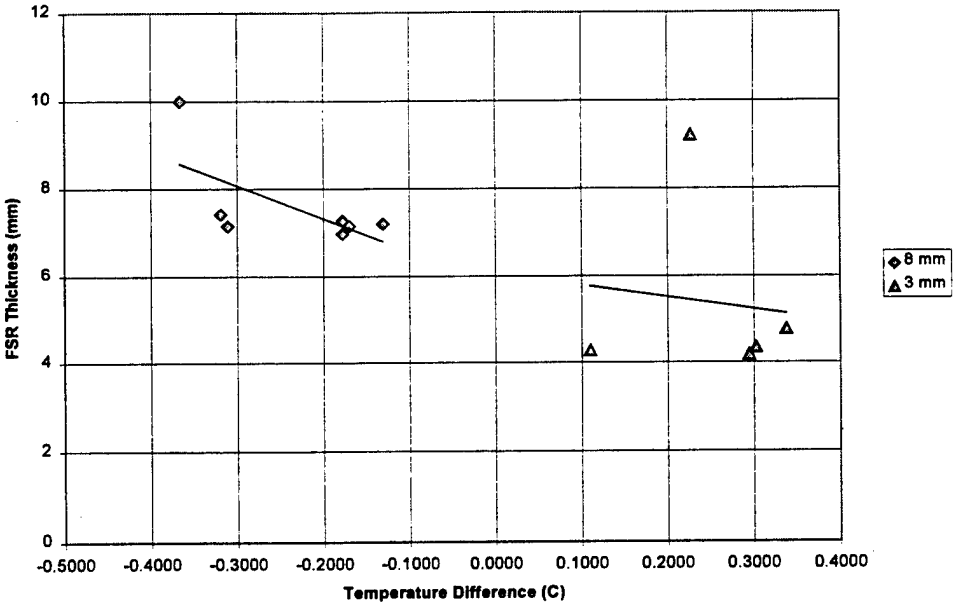

Figure A-10. Diesel Oils During Wave Conditions for Day 2 with "Good" or "Excellent" FSR Readings (12 September 1996)

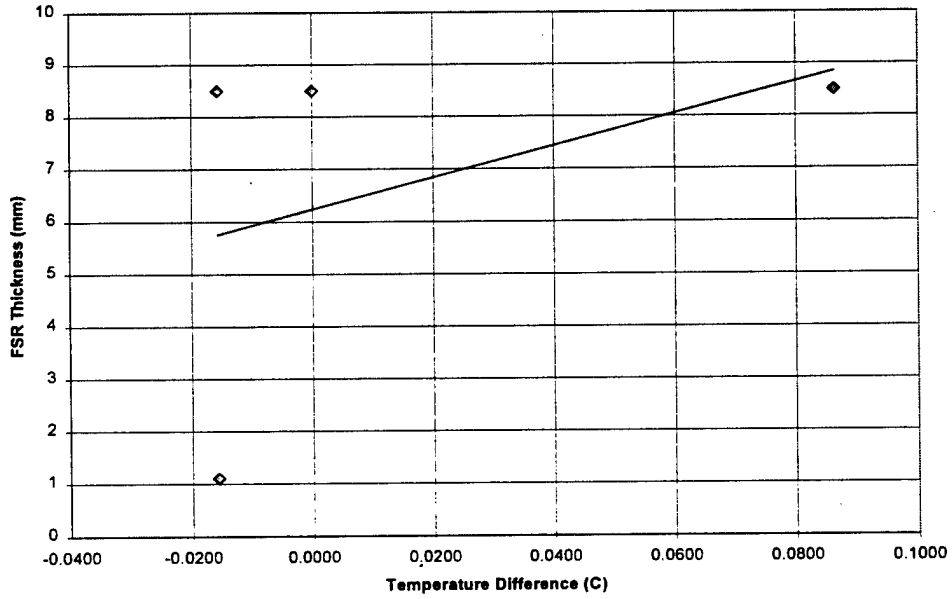

Figure A-11. 8 mm Diesel Oil During Chop Conditions for Day 2 (12 September 1996)

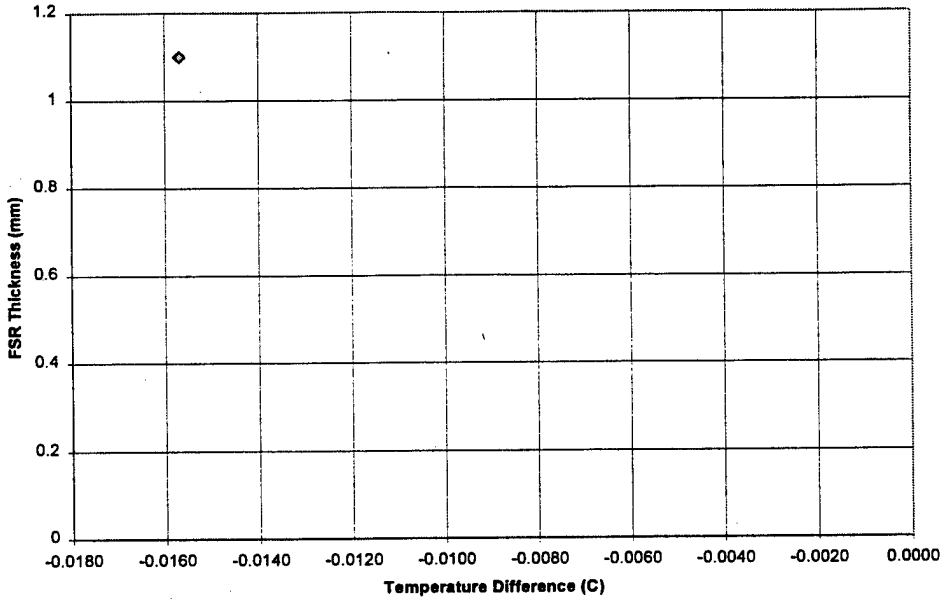

Figure A-12. 1 mm Diesel Oil During Chop Conditions for Day 2 with "Good" or "Excellent" FSR Readings (12 September 1996)

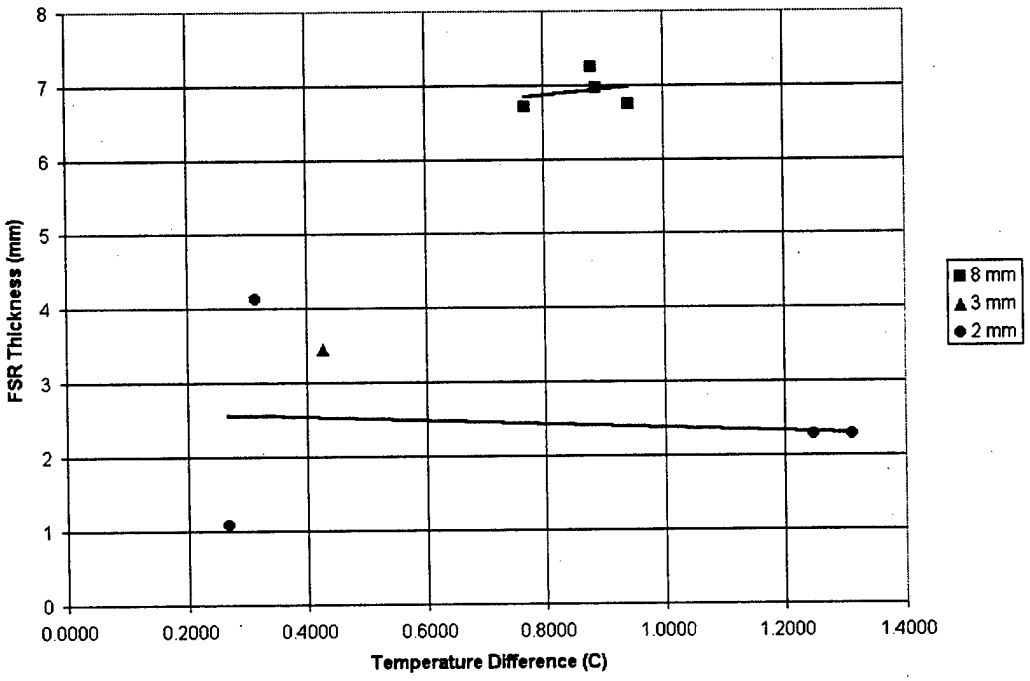

Figure A-13. All Crude Oils During Wave Conditions for Day 2 (12 September 1996)

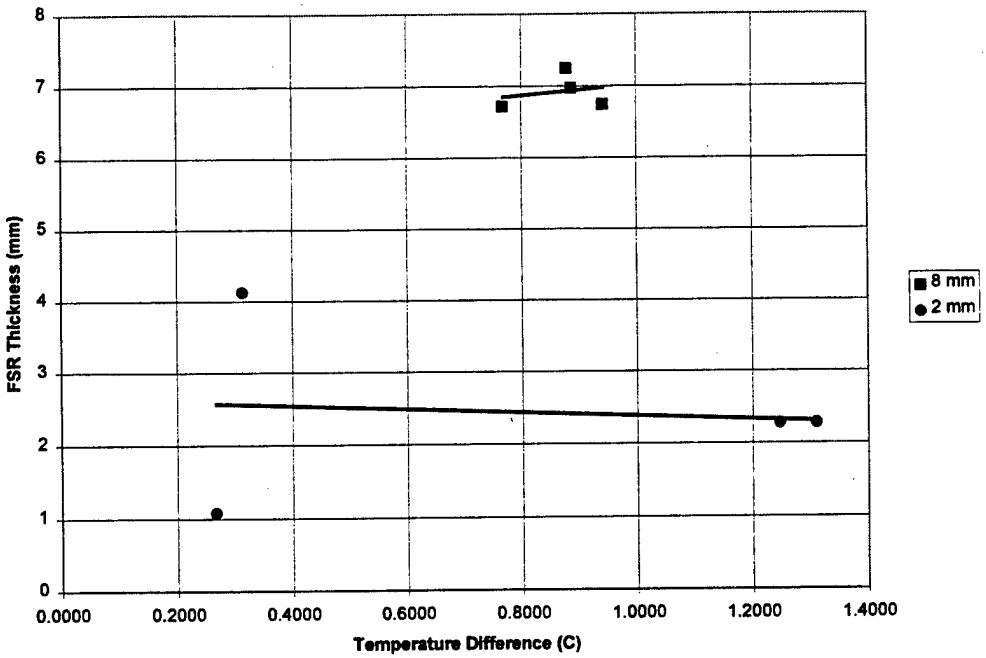

Figure A-14. Crude Oils During Wave Conditions for Day 2 with "Good" or "Excellent" FSR Readings (12 September 1996)

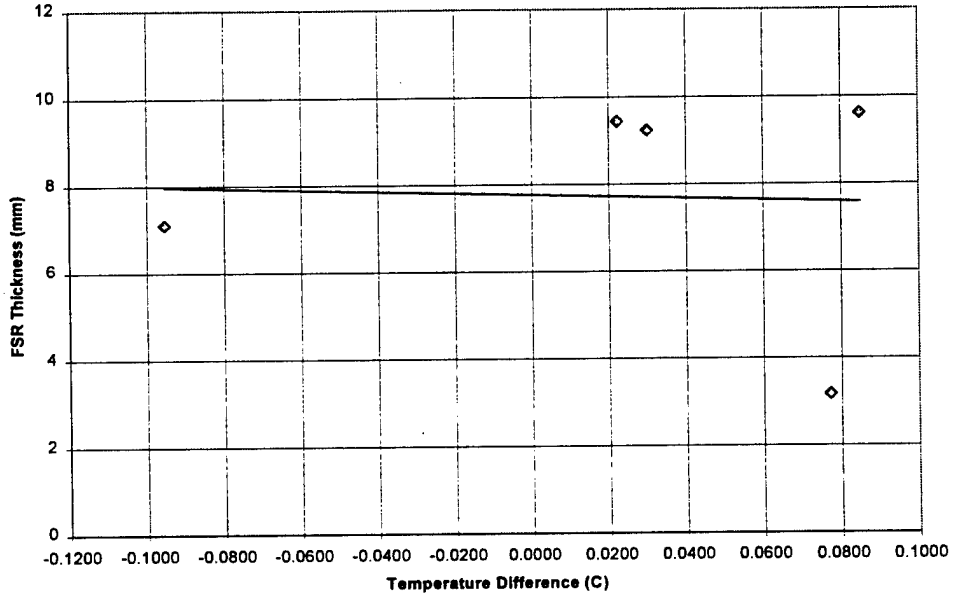

Figure A-15. 8 mm Crude Oils During Chop Condition 1 for Day 2 (12 September 1996)

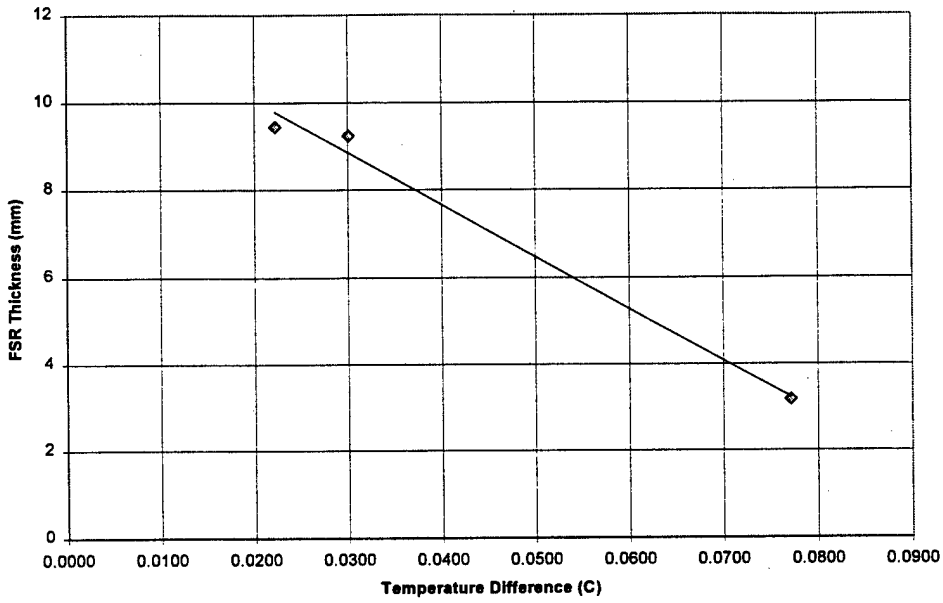

Figure A-16. 8mm Crude Oils During Chop Condition 2 for Day 2 with "Good" or "Excellent" FSR Readings (12 September 1996)

[BLANK]

APPENDIX B: INDIVIDUAL PLOTS OF OIL SLICKS

This appendix contains plots of FSR thickness versus IR temperature difference for each individual ring, organized by test period. As noted in Section 3.2 the abscissa on the plots in this appendix is temperature difference. This is the value of the observed oil temperature less the temperature of the adjacent water surface at the time of IR image acquisition, expressed in degrees Celsius. Linear trendlines show the relationship of the various FSR data points obtained from the same ring. The nominal oil thickness for each ring is cited in the figure caption. The plots are temporally ordered according to test series.

B.1 DRY RUN DAY

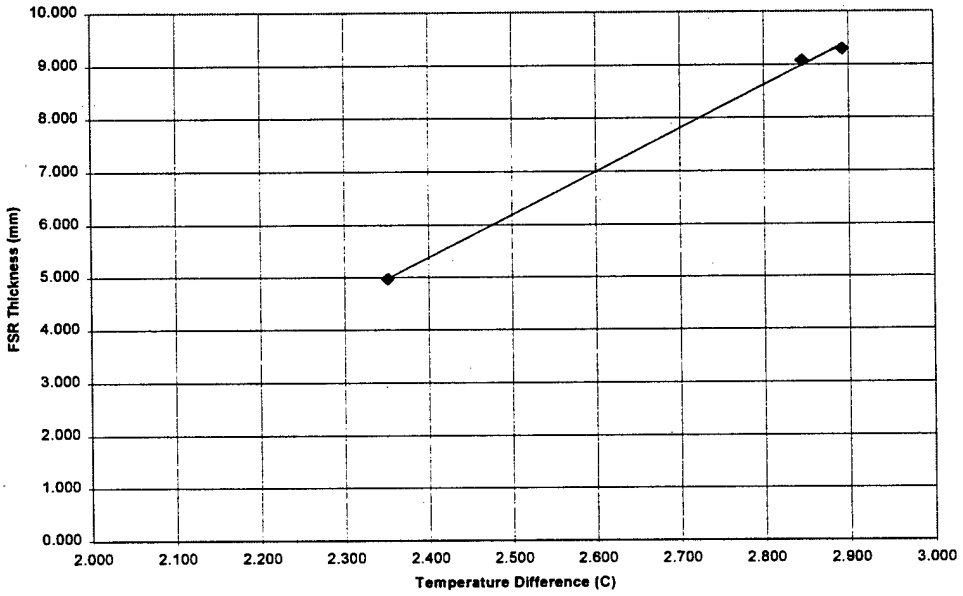

Figure B-1. 8 mm Diesel

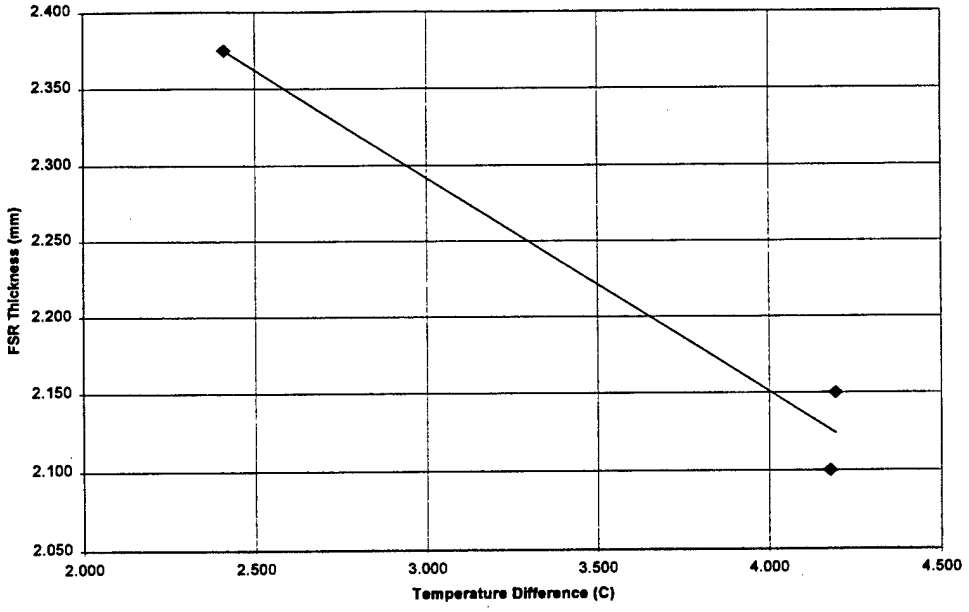

Figure B-2. 2 mm Waste

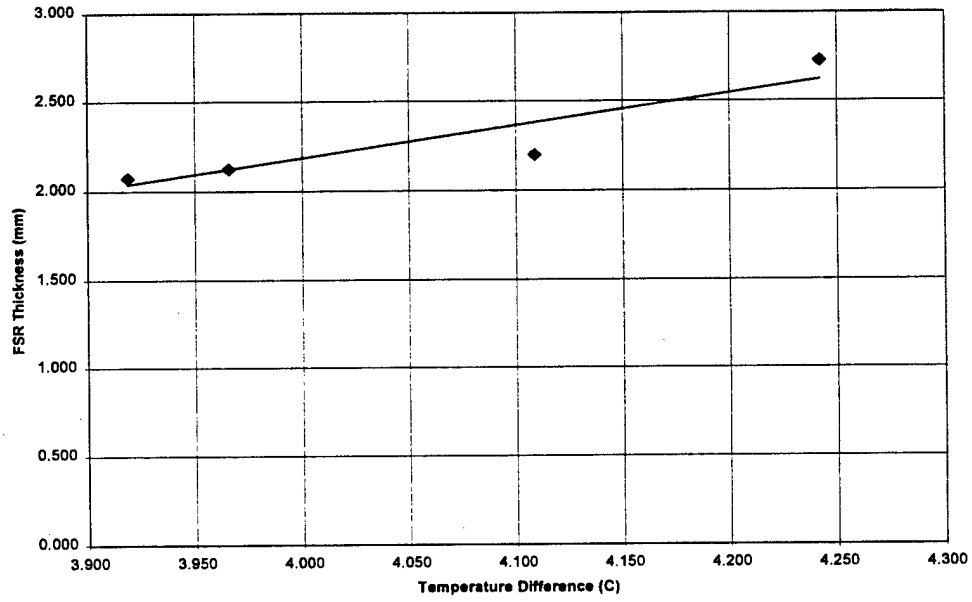

Figure B-3. 2 mm Diesel

B.2 DAY 1

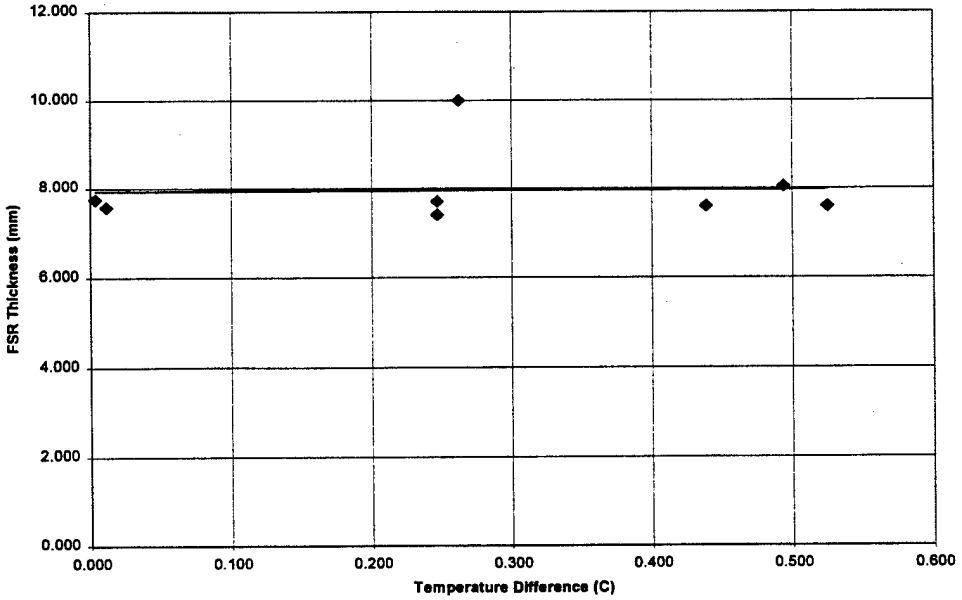

Figure B-4. 8 mm Diesel

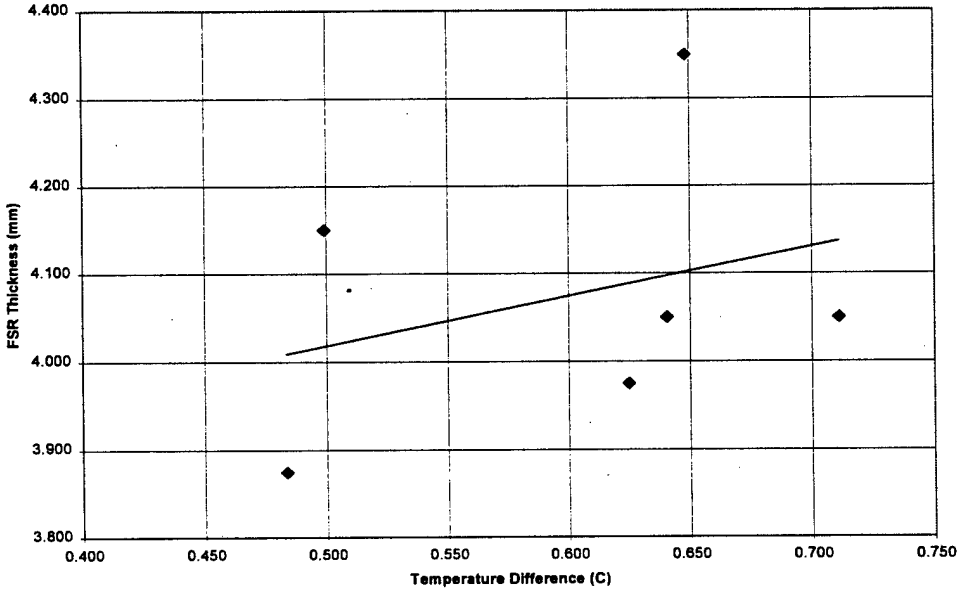

Figure B-5. 3 mm Diesel

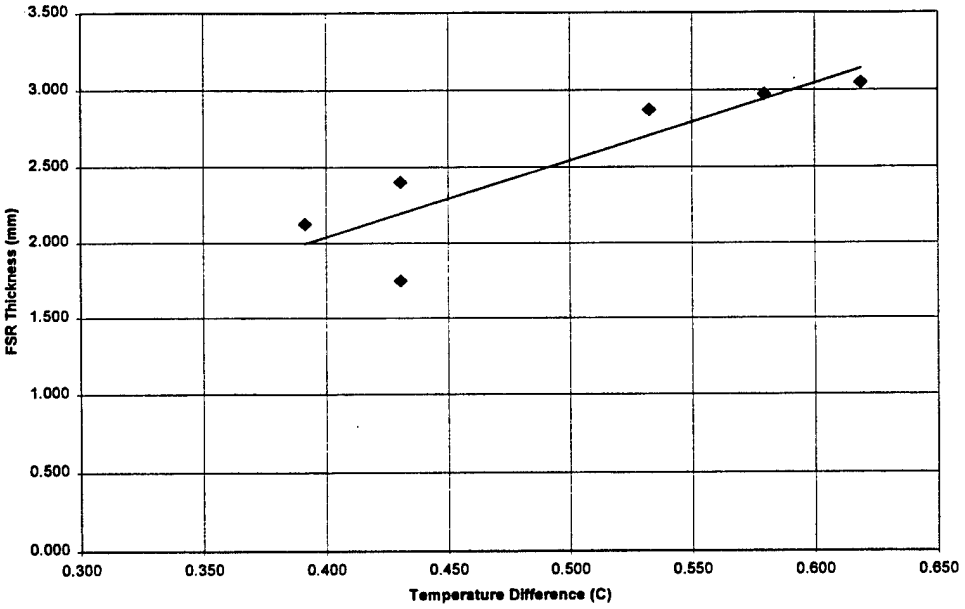

Figure B-6. 2 mm Diesel

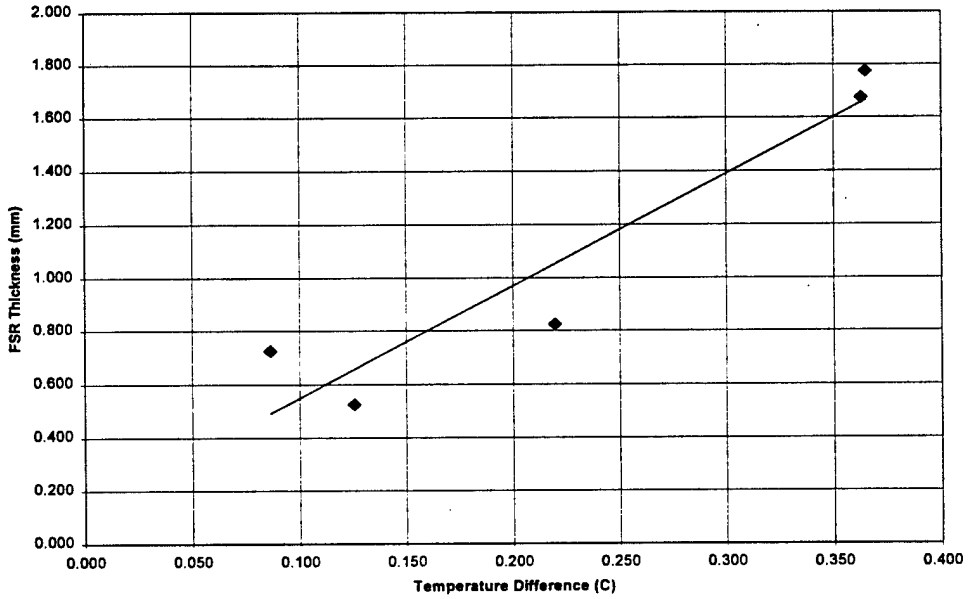

Figure B-7. 1 mm Diesel

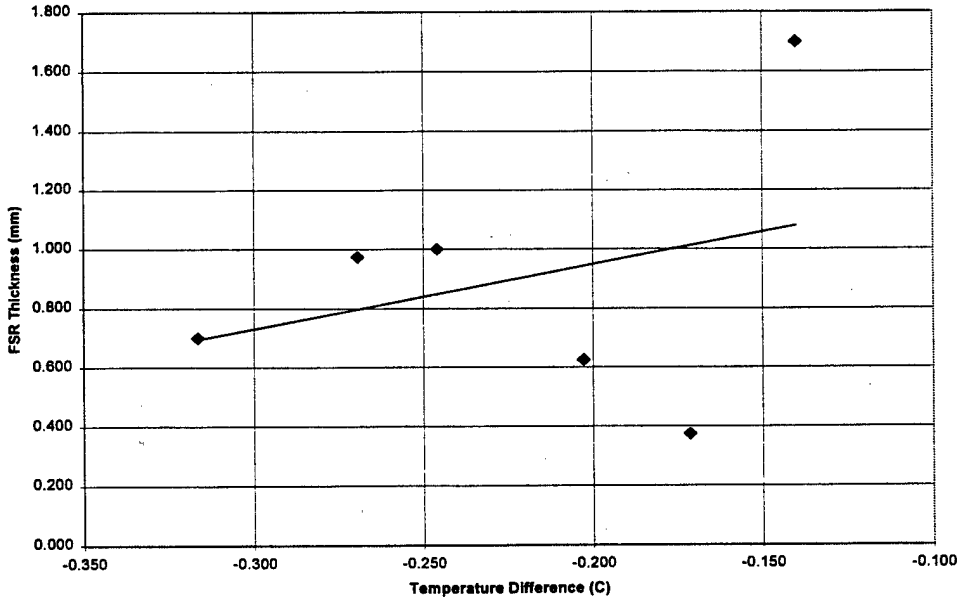

Figure B-8. 0.5 mm Diesel

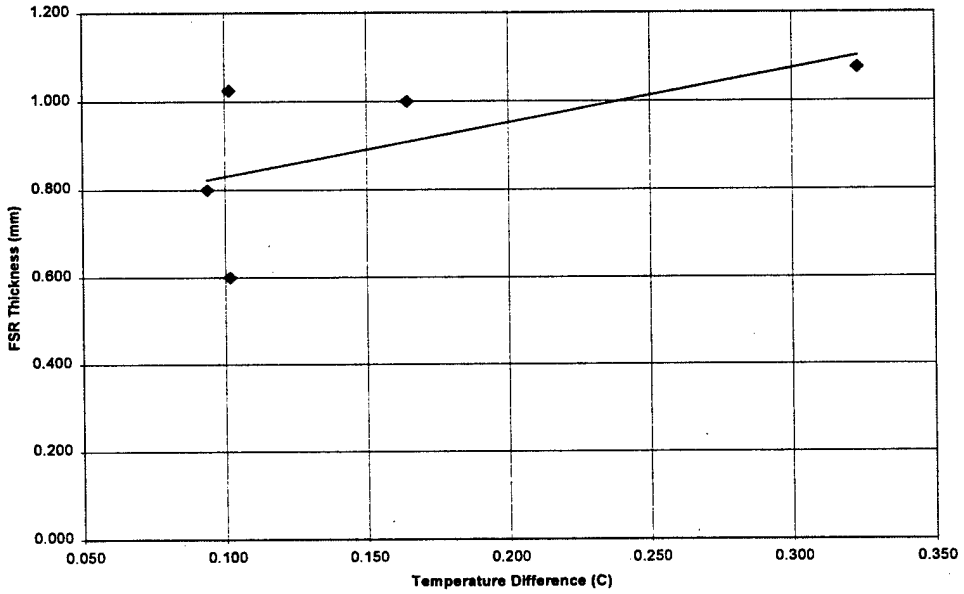

Figure B-9. Mixed Diesel and Sundex

B.3 NIGHT 1

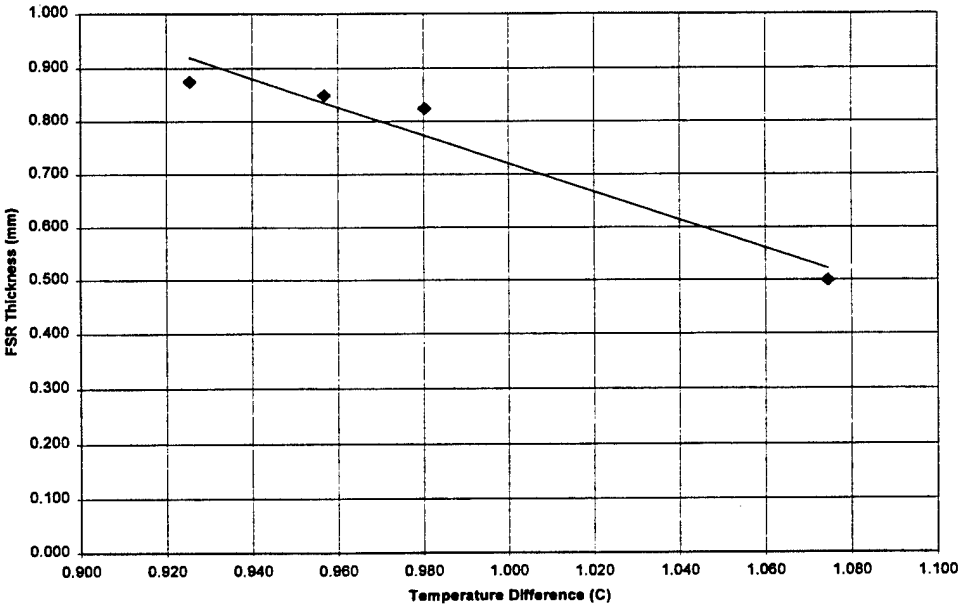

Figure B-10. 0.5 mm Crude

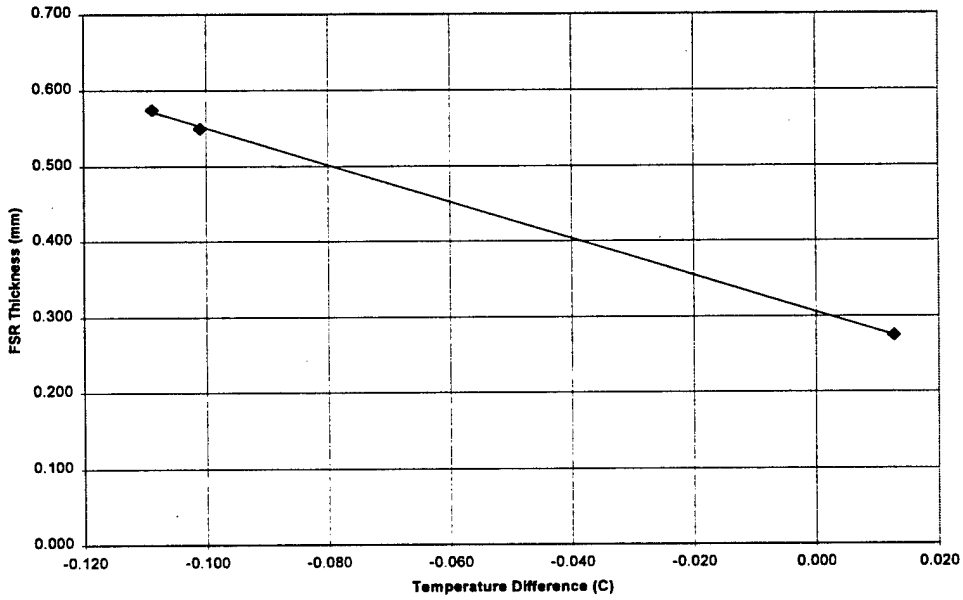

Figure B-11. 0.5 mm Diesel

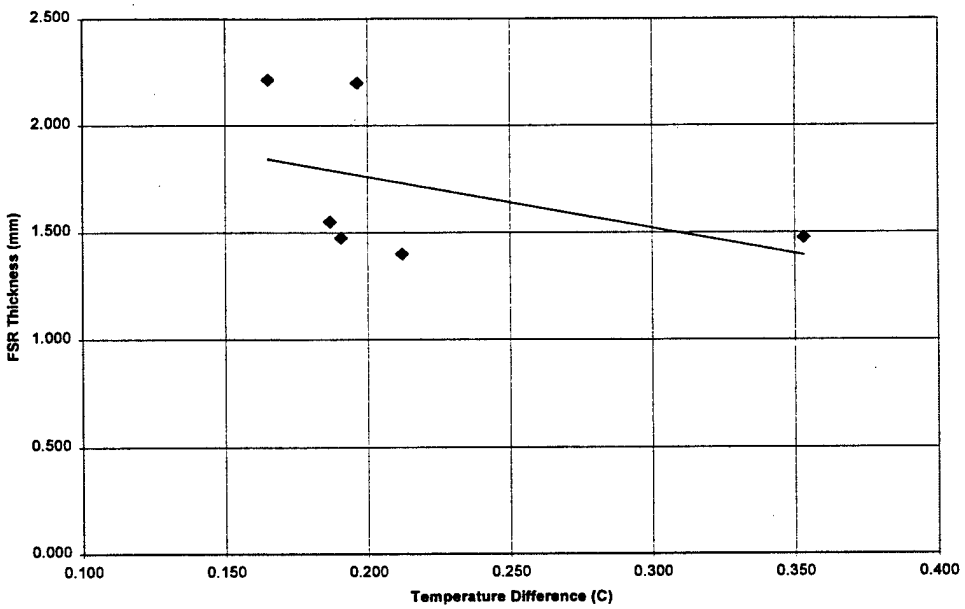

Figure B-12. 1 mm Crude

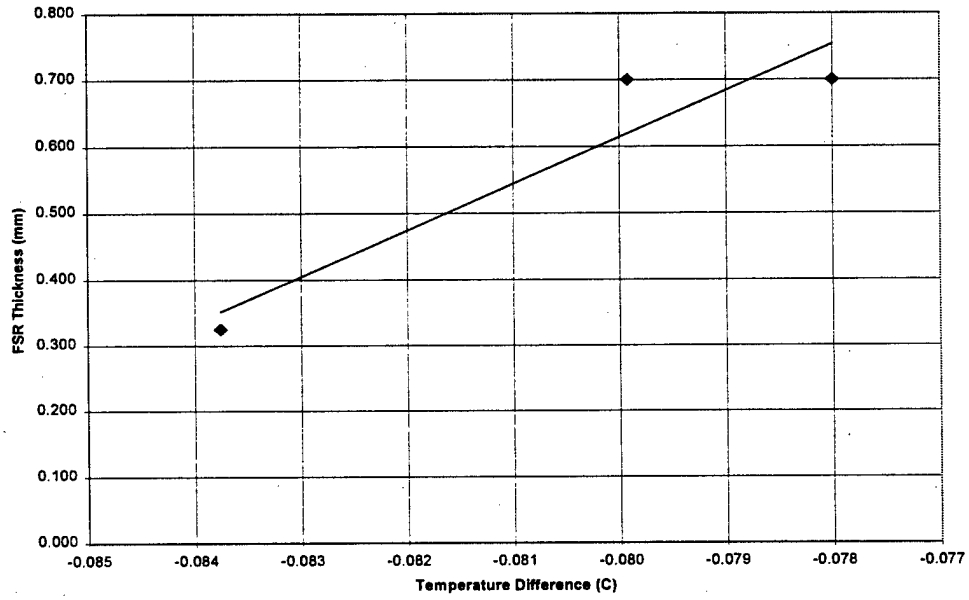

Figure B-13. 1 mm Diesel

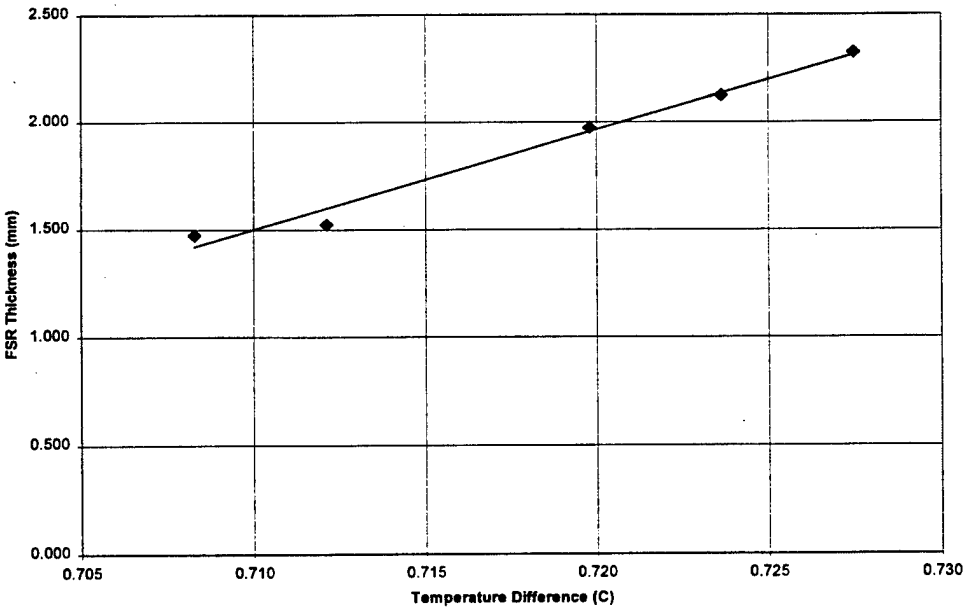

Figure B-14. 2 mm Crude

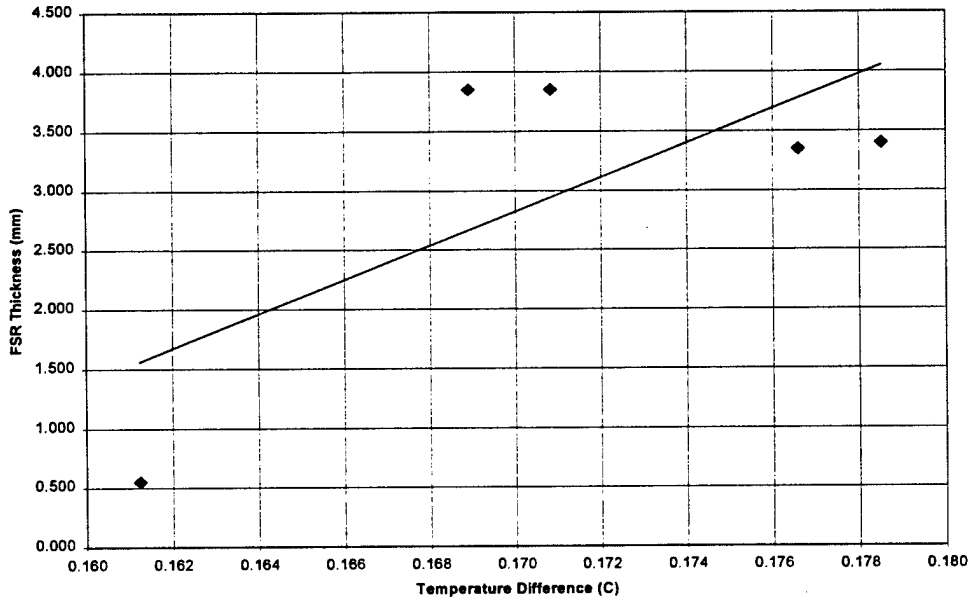

Figure B-15. 2 mm Diesel

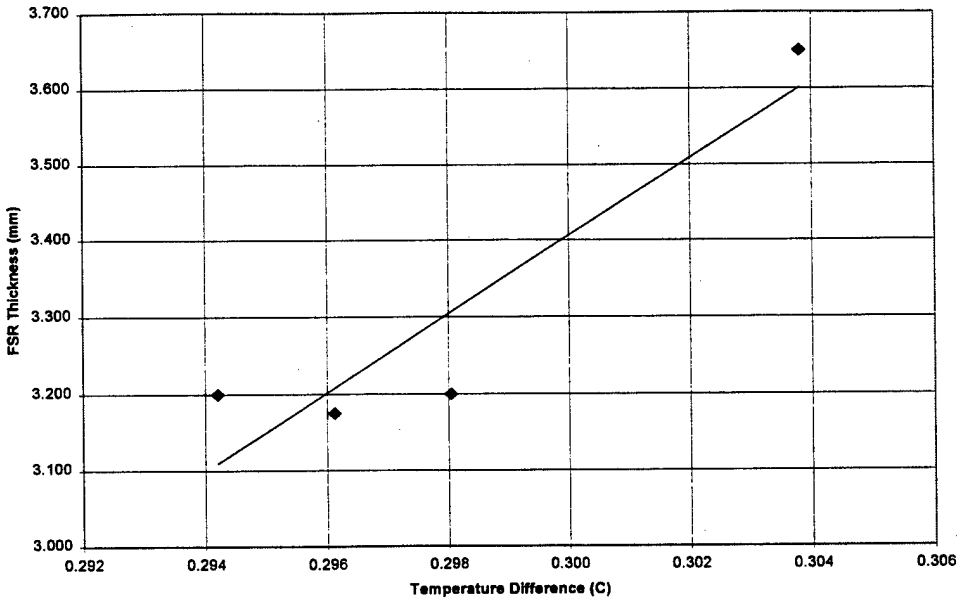

Figure B-16. 3 mm Crude

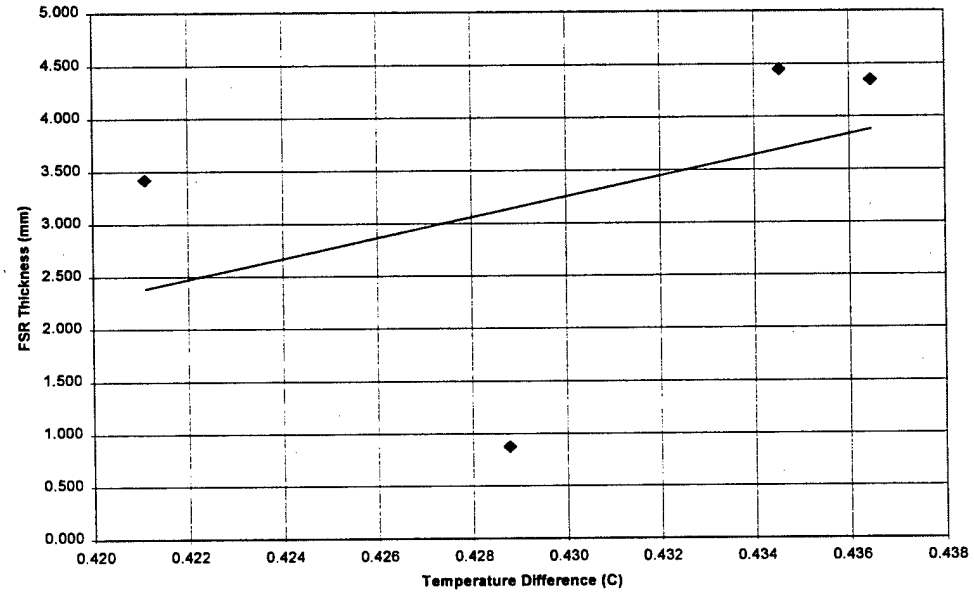

Figure B-17. 3 mm Diesel

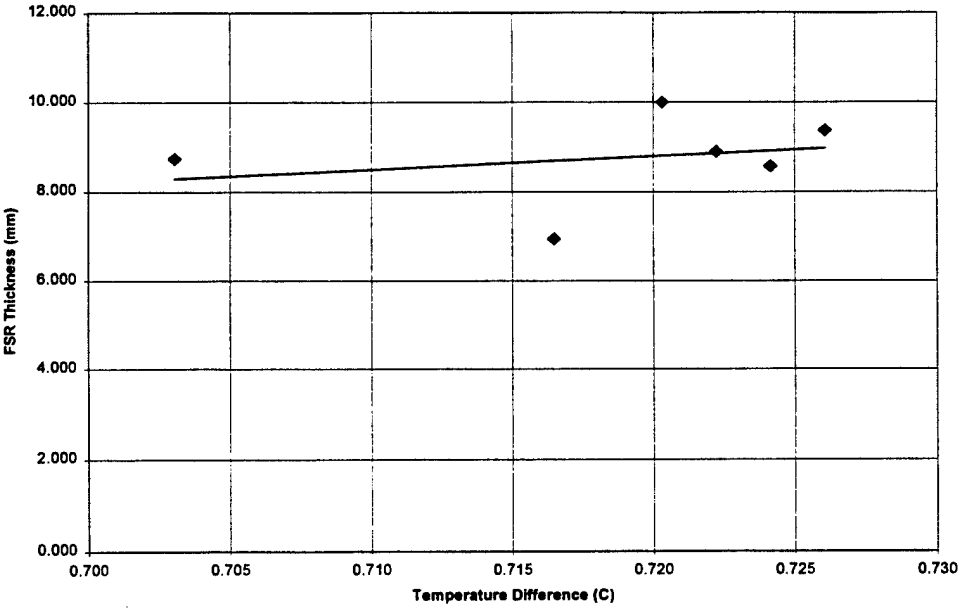

Figure B-18. 8 mm Crude

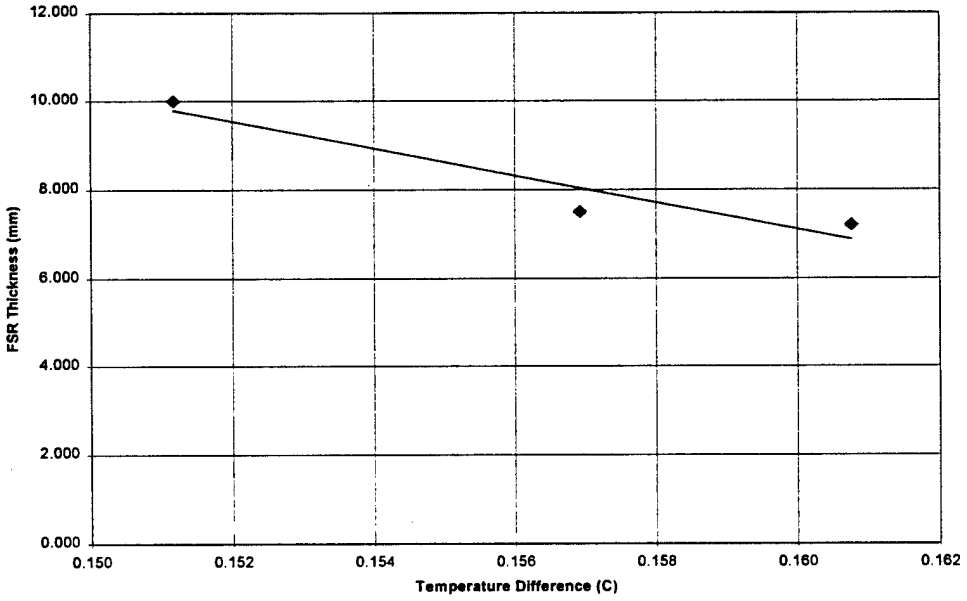

Figure B-19. 8 mm Diesel

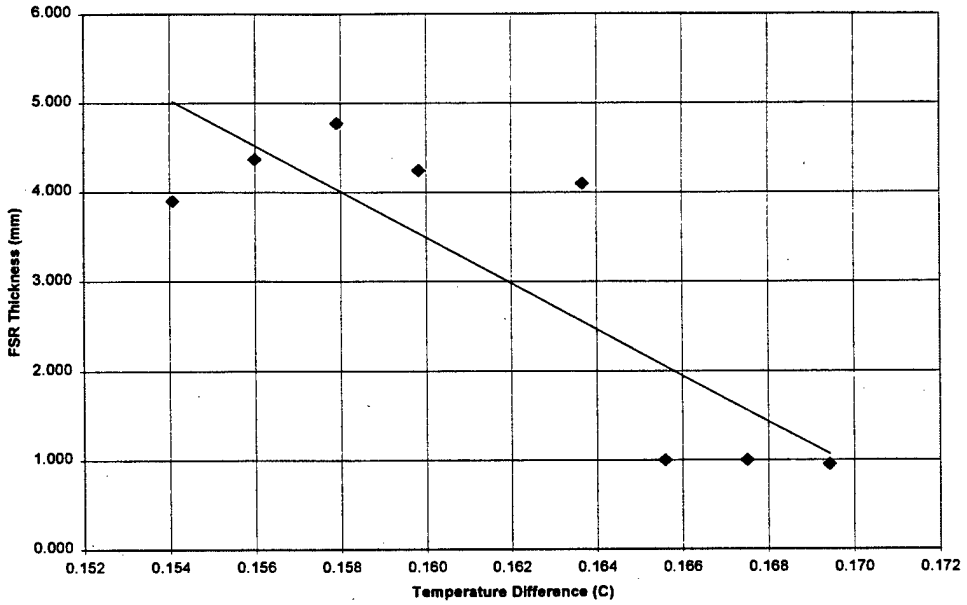

Figure B-20. 3 mm Diesel with Fans

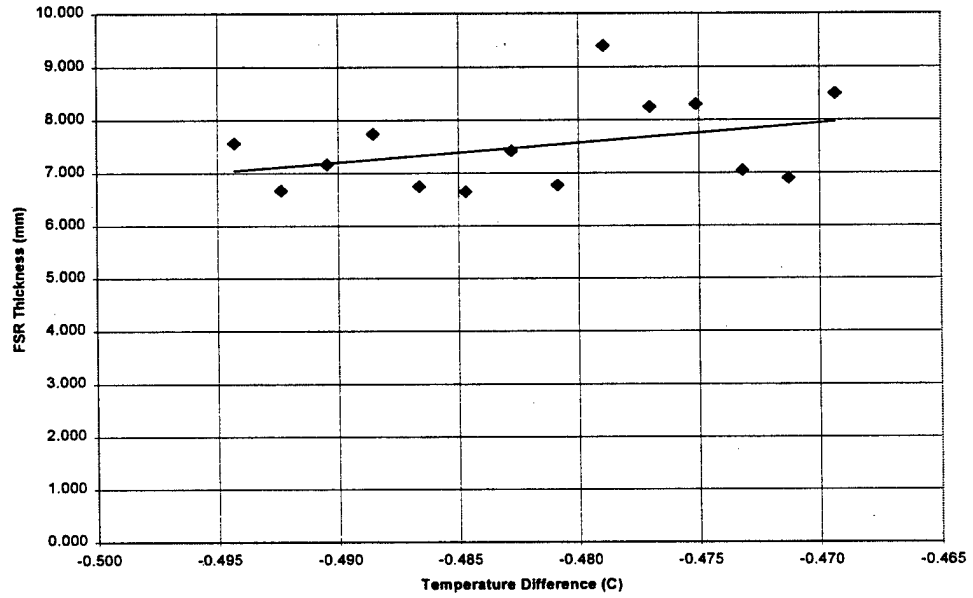

Figure B-21. 8 mm Diesel with Fans

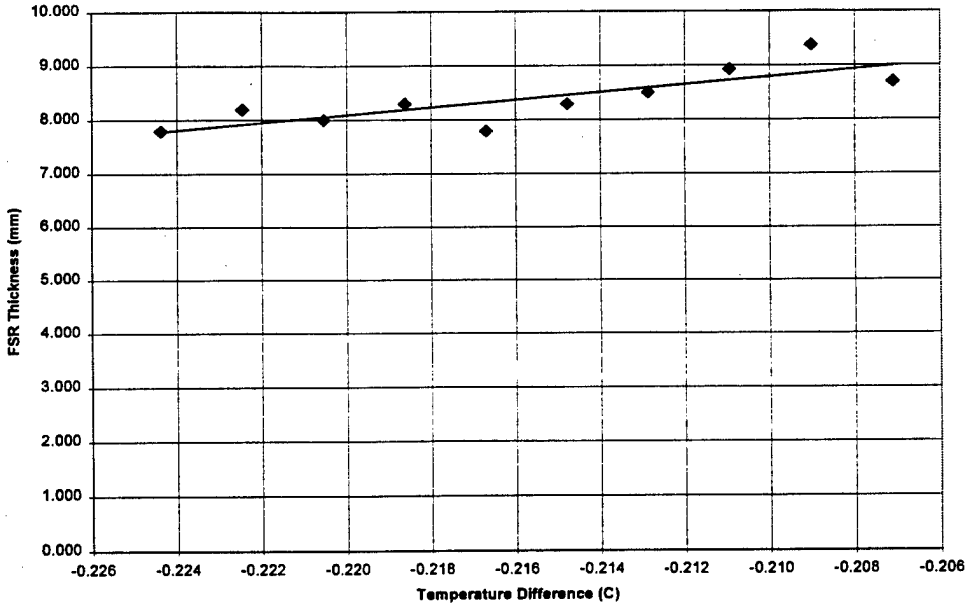

Figure B-22. 8 mm Crude with Fans

B.4 DAY 2

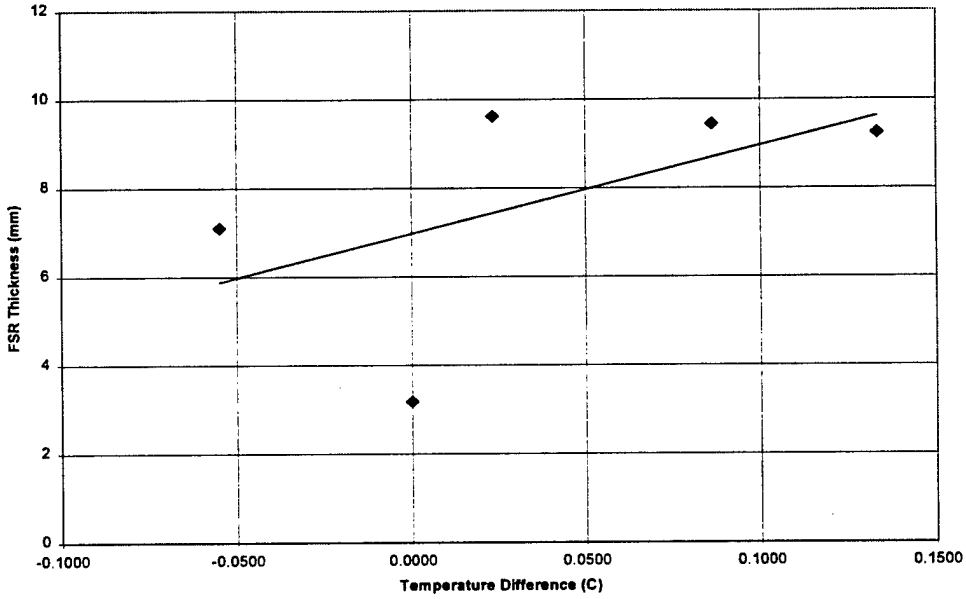

Figure B-23. 8 mm Crude with Harbor Chop

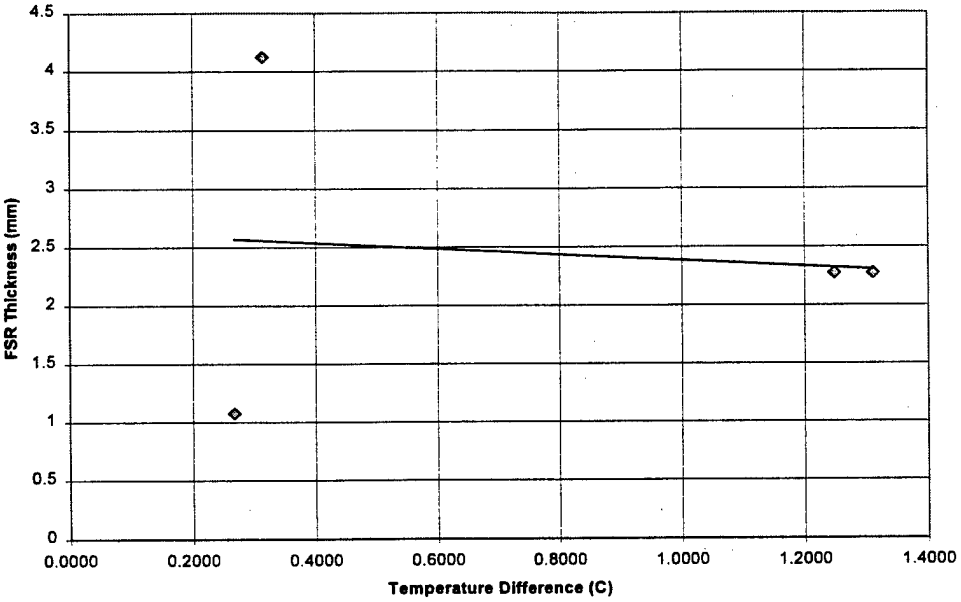

Figure B-24. 2 mm Crude with High Waves

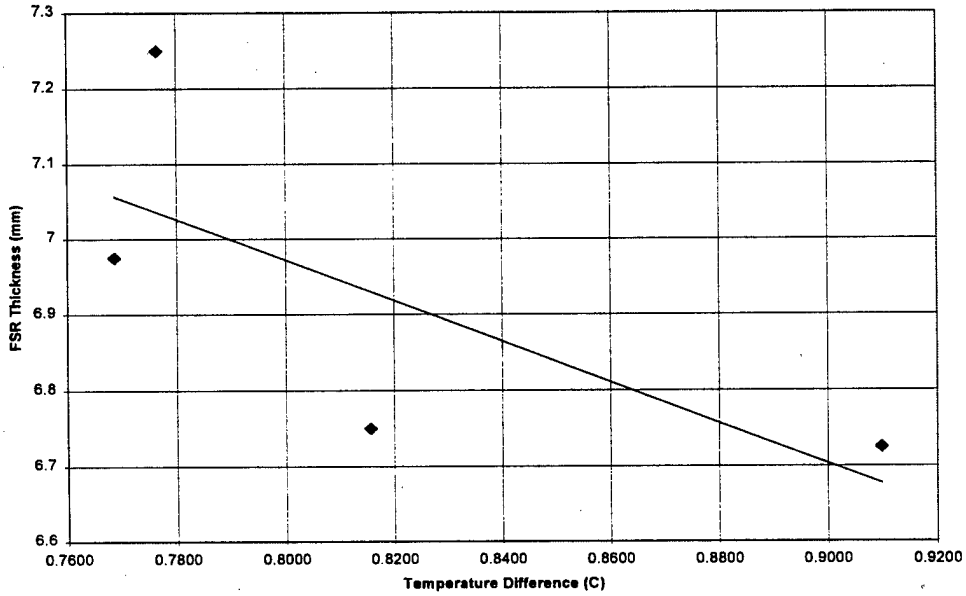

Figure B-25. 8 mm Crude with High Waves

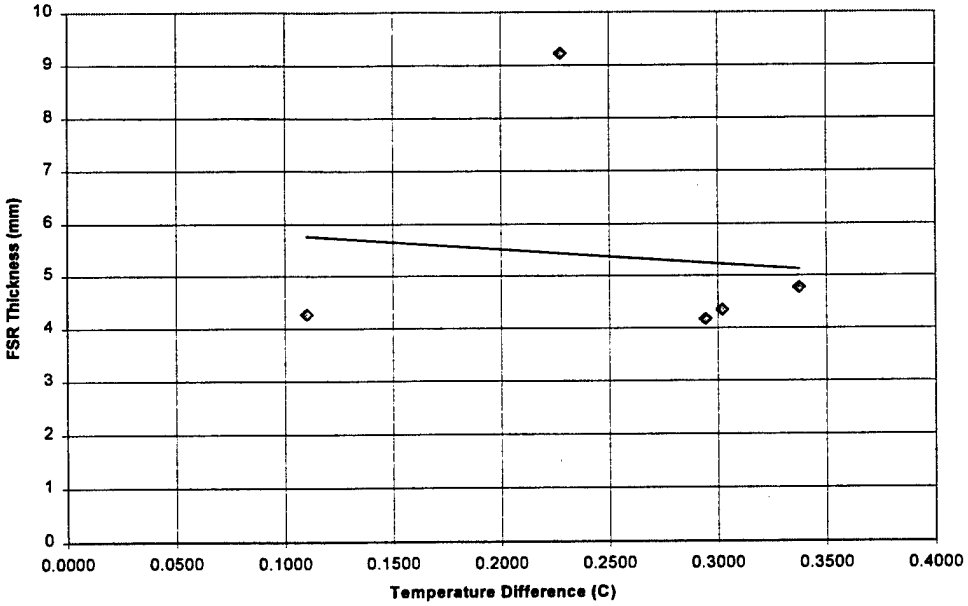

Figure B-26. 3 mm Diesel with High Waves

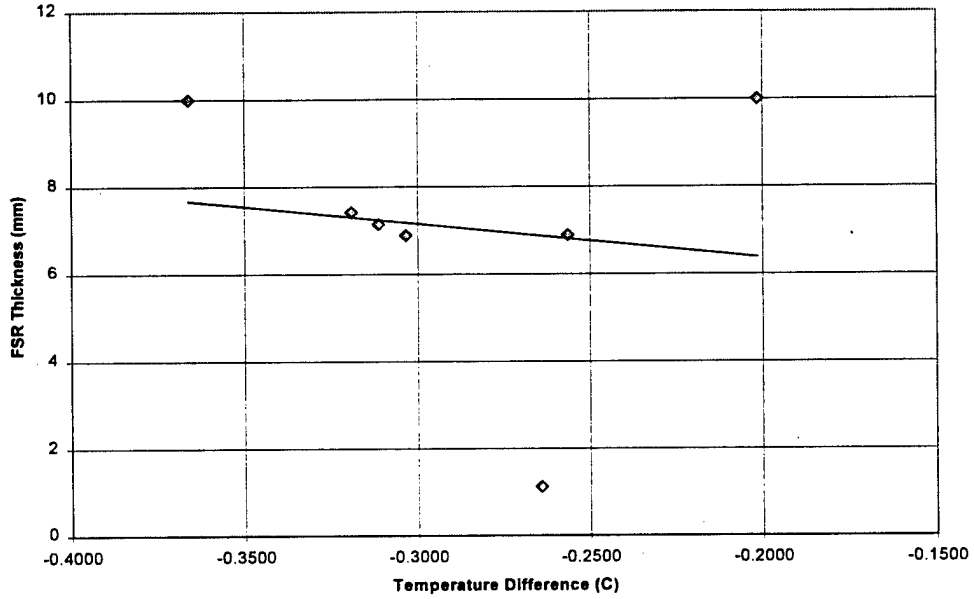

Figure B-27. 8 mm Diesel with High Waves

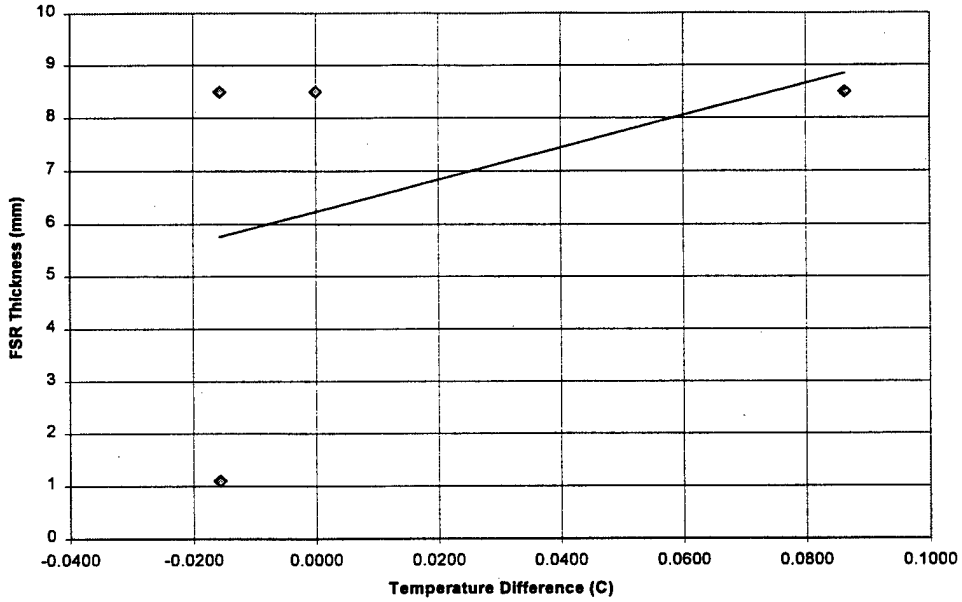

Figure B-28. 8 mm Diesel with Harbor Chop

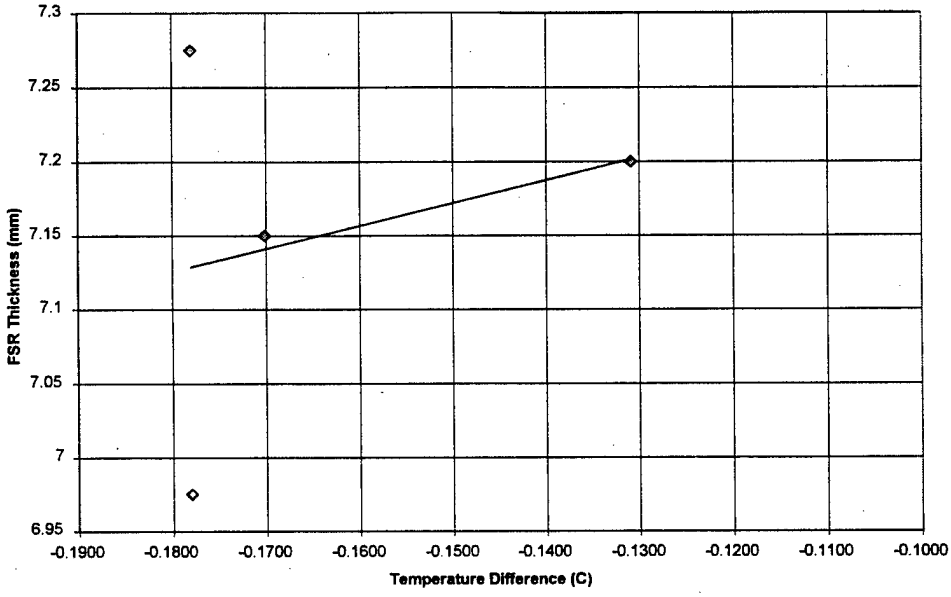

Figure B-29. 8 mm Diesel with Low Waves

B.5 DAY 3

Due to an equipment failure, the FSR was not available on Day 3. The available infrared data is presented in Section 3.2.5.